Geol. Mag. **143** (*1*), *2006, pp. 115–135.* © *2006 Cambridge University Press*
doi:10.1017/S0016756805001196 *Printed in the United Kingdom*

Geochemistry, mineral chemistry and petrogenesis of a Neoproterozoic dyke swarm in the north Eastern Desert, Egypt

M. DAWOUD*, H. A. ELIWA*§, G. TRAVERSA†, M. S. ATTIA* & T. ITAYA‡

*Geology Department, Faculty of Science, Minufiya University, Egypt
†Department of Earth Sciences, Roma 1 University, Italy
‡Research Institute of Natural Sciences, Okayama University of Science, 1-1 Ridai-cho, Okayama, 700 Japan

(*Received* 24 March 2005; *accepted* 24 May 2005)

Abstract – Dyke swarms traverse Neoproterozoic rocks in the Hawashiya region in the extreme northern part of the Eastern Desert of Egypt. They are a suite of basaltic andesite and andesite mafic dykes, and dacitic and rhyolitic felsic dykes. The mafic dyke suite is more abundant in the younger granites (577 ± 6 Ma) than in the older granitoids (614 Ma), in which the felsic dykes are the most common. The dyke swarms trend predominantly NE–SW, and the felsic dyke suite is older than the mafic dyke suite. Both dyke suites are calc-alkaline (alkaline dykes are rare) and are relatively poor in TiO_2 and Nb but enriched in the incompatible elements and HFSE. The felsic dyke suite is enriched in REE and is strongly LREE fractionated relative to the mafic dyke suite. Although the Hawashiya dykes were emplaced at the end of the Neoproterozoic era in an extensional tectonic setting, they have geochemical characteristics that are consistent with a subduction-related regime. These chemical signatures were inherited from the lithospheric rocks that produced their host Hawashiya granitoids. The felsic dyke suite magma may be derived from crustal rocks (essential source component) by partial melting. The mafic dyke suite magma was generated from a lithospheric mantle and has undergone fractional crystallization of plagioclase, amphibole, clinopyroxene and magnetite, as documented by major and trace elements fractionation modelling.

Keywords: Arabian–Nubian Shield, Neoproterozoic, Egypt, extension, lithosphere.

1. Introduction

The Arabian–Nubian Shield consists of a series of Neoproterozoic intra-oceanic island arcs that were assembled with various microplates and slivers of ophiolites between 870 and 600 Ma, and subsequently by intrusion of post-orogenic granitoids followed by uplift and cooling about 570–500 Ma ago (Greenwood *et al*. 1976; Pallister *et al*. 1988; Dixon & Golombek, 1988; Berhe, 1990). It covers an area of about 2600 kilometres length by 1000 kilometres width and includes the Nubian Shield (Egypt, Sudan and Ethiopia) to the west of the Red Sea and the Arabian Shield (Jordan, Saudi Arabia and Yemen) to the east of the Red Sea.

Precambrian rocks of Egypt constitute the extreme northwestern portion of the Arabian–Nubian Shield and crop out in the Eastern Desert and southern Sinai. On the basis of lithology and age, the basement rocks of the Eastern Desert of Egypt are subdivided into three distinctive structural domains: south Eastern Desert, central Eastern Desert and north Eastern Desert (Stern & Hedge, 1985), in order of decreasing age. The north Eastern Desert comprises large areas of calc-alkaline plutons, and numerous late Neoproterozoic (~ 580 Ma) post-kinematic pink granitoids, with intervening areas of Dokhan Volcanics with undeformed molasse-type sediments. Stern, Gottfried & Hedge (1984) defined four principal rock associations, making up nearly the entire basement in the north Eastern Desert, which include: (1) Hammamat Formation, (2) Dokhan Volcanics, (3) dykes and (4) epizonal granites and mesozonal granodiorite, which are the oldest rock types in the area. The Dokhan Volcanics and the Hammamat Formation developed in troughs extending parallel to the trend of the E–W to NE–SW compositionally bimodal dyke swarms (540 to 595 Ma) (Stern & Hedge, 1985). The lack of structural evidence for compression, along with evidence for rift-related sedimentation, bimodal igneous activity, subparallel dyke swarms and abundant passively emplaced A-type granite plutons support the conclusions of Stern, Gottfried & Hedge (1984) that the Late Precambrian crustal evolution of the north Eastern Desert occurred principally in a strongly extensional tectonic environment.

Schürmann (1966) was the first to document the abundance of the dykes in the north Eastern Desert. Stern & Hedge (1985) identified four magmatic events in the north Eastern Desert, of which the third event at 600–575 Ma represents the principal episode of extensional movement and dyke emplacement. The final event, at 550 Ma, comprises the emplacement of minor alkaline granites and dykes. The north Eastern Desert is traversed by several undeformed dyke swarms

§ Author for correspondence: eliwa98@yahoo.com

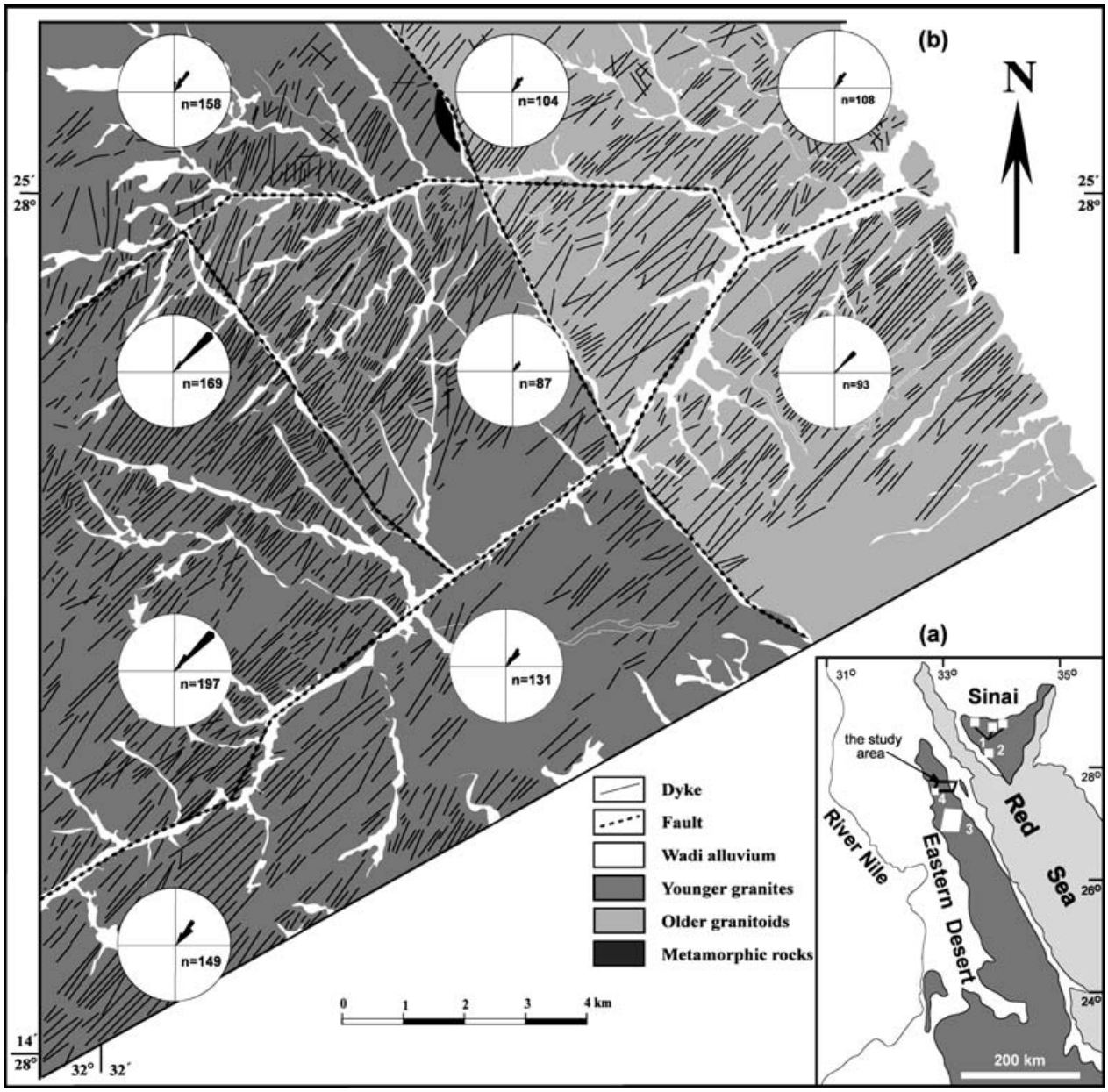

Figure 1. (a) Map shows the location of the study area and the occurrences of other dyke areas marked by the following numbers: 1 – West Southern Sinai dykes (Iacumin *et al*. 1998), 2 – East Southern Sinai dykes (Friz Töpfer, 1991), 3 – North Eastern Desert dykes (Stern, Sellers & Gottfried, 1988), 4 – G. Samr El-Qaa Volcanics (Eliwa, 2000). (b) Geological map of Wadi Hawashiya area, North Eastern Desert, Egypt. Rose diagrams show the abundance and directions of dykes.

(Vail, 1970), which emplaced during crustal extension (Stern, Gottfried & Hedge, 1984) about 600 Ma ago (Stern & Hedge, 1985; Stern & Voegeli, 1987).

The dyke swarms trend NE–SW, indicating NW–SE crustal extension related to strike-slip faulting along the NW–SE-directed Najd fault system (active between 620 and 540 Ma) in the northern part of the central Eastern Desert (Stern, 1985).

The aim of the present study is to throw light on the geochemical characteristics, probable source rocks, and genetic relationships with host granitoids as well as the petrogenetic processes responsible for the evolution of north Eastern Desert dykes. The main reason for selecting this area is the abundance of dyke swarms, in addition to absence of previous detailed mapping and geochemical studies.

2. Regional geology

The investigated area is bordered on the east by the Red Sea coastal plain and on the west by sedimentary rocks probably of Cretaceous age (El-Ramly & Hermina, 1978).

The Wadi Hawashiya area is mostly covered by older and younger granitoids (Fig. 1). The abundance of dyke

swarms is the conspicuous feature in the study area. The dyke swarms are numerous (~3 % of the region), while individual dykes reach up to 30 m in width and up to 10 km in length. Dykes are always parallel or sub-parallel and some have quenched margins and are coarse-grained in the centre. In some regions, the felsic dykes are thicker than the mafic dykes. Mafic dykes are more abundant in the younger granites (577 ± 6 Ma: Stern & Hedge, 1985) than in the older granitoids (614 Ma: Stern & Hedge, 1985), while the older granitoids are traversed by abundant felsic dykes. Most dykes exhibit sharp contacts against their host rocks. In the younger granites, some felsic dykes were found within the mafic dyke swarms and either run parallel to or are cut by them. In general, the mafic dykes are younger than the felsic ones, as has been noted by Hassan & Hashad (1990). In the younger granites, especially near the contact with the older granitoids, mafic dykes are present but felsic dykes are absent. Composite dykes with felsic cores and mafic to intermediate margins are not uncommon in the older granitoids and have the same composition as similar individual dykes. It appears that most felsic dykes were emplaced either before or during the intrusion of the younger granites.

Although some dykes extend for several kilometres and vary in width from 0.50 m up to 30 m, no change in colour, grain size, mineral assemblage or texture was observed along strike.

3. Structural features

Distribution and azimuth rose diagrams for the studied dykes are shown in Figure 1. All dykes trend NE–SW and dip steeply to vertical (90–75°) (Fig. 1). Dykes trend N45° E in most areas, but in a few areas in the southern parts they become N52° E. The average spacing between dykes, measured at right angles to their trend, is smaller in the younger granites than in the older granitoids. The dykes show no tendency to be confined by an envelope oblique to their trend as would be expected if these dykes formed in response to Riedel shears. There are quite a few examples of dykes intruding other dykes without displacement of either, which also argues against the dykes being emplaced along shears. The bifurcation of the dykes could suggest that the dykes occupy pure tensional fractures. The very steep orientation of the dykes, absence of evidence for displacement across them, and their bifurcating morphology suggest the dykes have intruded in response to a subhorizontal NW–SE crustal extension.

4. Petrography

Petrographically, the dykes can be classified into basaltic andesites, andesites, dacites and rhyolites.

Basaltic andesites are mainly aphyric, with textural variations including intersertal, subophitic and rarely doleritic types. Phenocrysts of plagioclase, hornblende and clinopyroxene are embedded in a very fine-grained groundmass of plagioclase laths, fine hornblende prisms, and some biotite and augite crystals. Accessories are opaques, while chlorite, actinolite, sericite and titanite are the secondary minerals. Plagioclase is mainly andesine in composition but varies from labradorite to oligoclase. Hornblende forms euhedral to subhedral microphenocrysts as well as small prisms in the groundmass and shows variable degrees of alteration to pale yellowish green to green chlorite. Clinopyroxene forms subhedral equant microphenocrysts.

Andesites are commonly porphyritic and consist of plagioclase, hornblende, and subordinate amounts of clinopyroxene, quartz and biotite phenocrysts. Accessories are opaques and apatite. Sericite, kaolinite, chlorite and epidote are the secondary minerals. Plagioclase is mainly andesine but ranges from labradorite to albite and forms subhedral tabular phenocrysts, variably altered to sericite and kaolinite. Hornblende forms subhedral to euhedral, elongated phenocrysts that are simply twinned. Some phenocrysts are corroded and embayed by intersertal textured groundmass consisting of quartz, plagioclase laths and few augite, hornblende and biotite crystals.

Dacites consist of plagioclase, biotite and minor perthite and quartz phenocrysts in a fine-grained groundmass. Common accessories are opaques and apatite, while zircon is rare. Kaolinite, chlorite and sericite are the secondary minerals. Plagioclase is oligoclase and forms subhedral to euhedral phenocrysts that are mostly zoned. Perthite is slightly kaolinitized. Biotite forms subhedral to anhedral flakes that are partially altered to chlorite with fine grains of opaques and titanite. Granophyric and sometimes myrmekitic intergrowths are characteristic of the groundmass composed of quartz, K-feldspar and minor biotite.

Rhyolites are aphyric to rarely porphyritic and comprise K-feldspar and quartz with minor plagioclase laths and biotite. Plagioclase is albite and sometimes forms glomeroporphyritic microphenocrysts. Biotite occurs as strongly pleochroic flakes. Microspherulitic intergrowths are common in a groundmass composed of K-feldspar and quartz. Alteration products are kaolinite and chlorite.

5. Analytical methods

All chemical analyses were carried out at Centro Di Studio per Equilibri Sperimentali in Minerali E Rocce Del C.N.R. c/o Dipartimento Di Science Della Terra, Universita Degli, Studi Di Roma, La Sapienza, Italy. Major and some trace elements and REE (nine samples) in 27 samples were analysed by X-ray fluorescence (XRF), using a Philips PW 1450 automatic spectrometer following the techniques of Norrish & Hutton

Table 1. Representative mineral chemistry of pyroxenes from Wadi Hawashiya dykes

Rock type	Basaltic andesites							Andesites									
Sample no.	200	200	212	212	212	212	212	254	254	254	254	254	254	254	268	268	268
Analysis	Cpx4-3	Cpx4-1	Cpx4-1	Cpx4-1	Cpx4-1	Cpx4-1	Cpx4-5	Cpx1-1	Cpx1-2	Cpx1-3	Cpx1-1	Cpx1-3	Cpx1-5	Cpx1-8	Cpx4-1	Cpx4-1	Cpx4-1
SiO_2	48.19	50.94	49.79	47.71	53.49	51.41	48.56	52.75	49.96	50.57	51.33	49.84	49.31	55.02	50.71	51.16	50.60
TiO_2	0.92	0.51	0.85	1.40	0.14	0.61	0.66	0.52	0.64	1.78	0.45	0.53	0.52	0.03	0.51	0.46	0.35
Al_2O_3	4.59	1.93	3.87	6.10	1.22	2.21	4.52	1.91	3.13	1.96	2.08	2.83	3.53	0.35	1.90	1.86	1.30
FeO	8.45	10.12	10.72	10.50	12.30	9.22	7.25	8.56	8.55	9.07	8.95	8.64	8.42	5.14	9.21	9.50	9.18
MnO	0.15	0.27	0.21	0.19	0.33	0.37	0.12	0.15	0.12	0.12	0.19	0.17	0.17	0.25	0.33	0.36	0.34
MgO	14.42	15.81	14.85	13.68	16.06	16.16	15.03	16.99	16.99	16.18	15.57	16.92	15.83	22.36	13.55	14.37	13.58
CaO	21.21	19.09	18.55	20.07	13.96	19.81	21.98	18.42	18.42	18.56	20.14	19.68	20.81	14.45	22.10	20.88	23.40
Na_2O	0.30	0.28	0.27	0.43	0.23	0.25	0.33	0.35	0.36	0.31	0.34	0.36	0.38	0.09	0.69	0.60	0.58
K_2O	0.01	0.00	0.02	0.06	0.04	0.01	0.01	0.00	0.01	0.02	0.07	0.00	0.02	0.02	0.04	0.04	0.00
Total	98.24	98.95	99.13	100.14	97.77	100.05	98.46	99.65	98.18	98.57	99.12	98.97	98.99	97.71	99.04	99.23	99.33
Numbers of cations on the basis of 6 oxygens																	
Si	1.813	1.907	1.867	1.772	2.038	1.899	1.813	1.946	1.865	1.899	1.913	1.847	1.831	2.019	1.903	1.913	1.895
Al^{iv}	0.187	0.085	0.133	0.228	0.000	0.096	0.187	0.054	0.135	0.087	0.087	0.123	0.154	0.000	0.084	0.082	0.057
Fe^{3+}	0.000	0.008	0.000	0.000	0.000	0.005	0.000	0.000	0.000	0.014	0.000	0.030	0.015	0.000	0.013	0.005	0.048
Sum T	2.000	2.000	2.000	2.000	2.038	2.000	2.000	2.000	2.000	2.000	2.000	2.000	2.000	2.019	2.000	2.000	2.000
Al^{vi}	0.017	0.000	0.038	0.039	0.055	0.000	0.011	0.029	0.003	0.000	0.005	0.000	0.000	0.015	0.000	0.000	0.000
Ti	0.026	0.014	0.024	0.039	0.004	0.017	0.019	0.014	0.018	0.050	0.013	0.015	0.015	0.001	0.014	0.013	0.010
Fe^{3+}	0.139	0.084	0.068	0.144	0.000	0.086	0.163	0.021	0.123	0.025	0.084	0.149	0.166	0.000	0.120	0.106	0.127
Fe^{2+}	0.009	0.019	0.041	0.021	0.029	0.008	0.000	0.001	0.000	0.020	0.033	0.000	0.000	0.000	0.108	0.080	0.105
Mg	0.809	0.882	0.830	0.757	0.912	0.890	0.807	0.934	0.857	0.906	0.865	0.836	0.818	0.984	0.758	0.801	0.758
Sum M1	1.000	0.999	1.001	1.000	1.000	1.001	1.000	0.999	1.001	1.001	1.000	1.000	0.999	1.000	1.000	1.000	1.000
Fe^{2+}	0.118	0.205	0.228	0.162	0.363	0.186	0.064	0.242	0.144	0.226	0.162	0.089	0.080	0.158	0.049	0.107	0.008
Mg	0.000	0.000	0.000	0.000	0.000	0.000	0.029	0.000	0.089	0.000	0.000	0.099	0.058	0.239	0.000	0.000	0.000
Mn	0.005	0.009	0.007	0.006	0.011	0.012	0.004	0.005	0.004	0.004	0.006	0.005	0.005	0.008	0.010	0.011	0.011
Ca	0.855	0.766	0.745	0.799	0.570	0.784	0.879	0.728	0.737	0.747	0.804	0.781	0.828	0.568	0.889	0.837	0.939
Na	0.022	0.020	0.020	0.031	0.017	0.018	0.024	0.025	0.026	0.023	0.025	0.026	0.027	0.006	0.050	0.044	0.042
K	0.000	0.000	0.001	0.003	0.002	0.000	0.000	0.000	0.000	0.001	0.003	0.000	0.001	0.001	0.002	0.002	0.000
Sum M2	0.882	0.795	0.773	0.839	0.600	0.814	0.936	0.758	0.856	0.775	0.838	0.911	0.919	0.822	0.951	0.894	0.992
WO	44.20	38.80	38.85	42.30	30.24	39.79	45.18	37.70	37.72	38.47	41.15	39.28	46.27	29.03	45.66	42.99	47.06
EN	41.81	44.71	43.28	40.11	48.40	45.17	42.99	48.38	48.41	46.66	44.27	46.99	48.97	62.51	38.95	41.16	38.00
FS	13.99	16.49	17.87	17.59	21.36	15.04	11.83	13.92	13.86	14.87	14.58	13.73	4.76	8.46	15.39	15.85	14.95

Sum T – sum of cations in tetrahedron site; Sum M1 – sum of cations in octahedron M1 site; Sum M2 – sum of cations in octahedron M2 site. Wo – wollastonite; En – enstatite; Fs – ferrosalite.

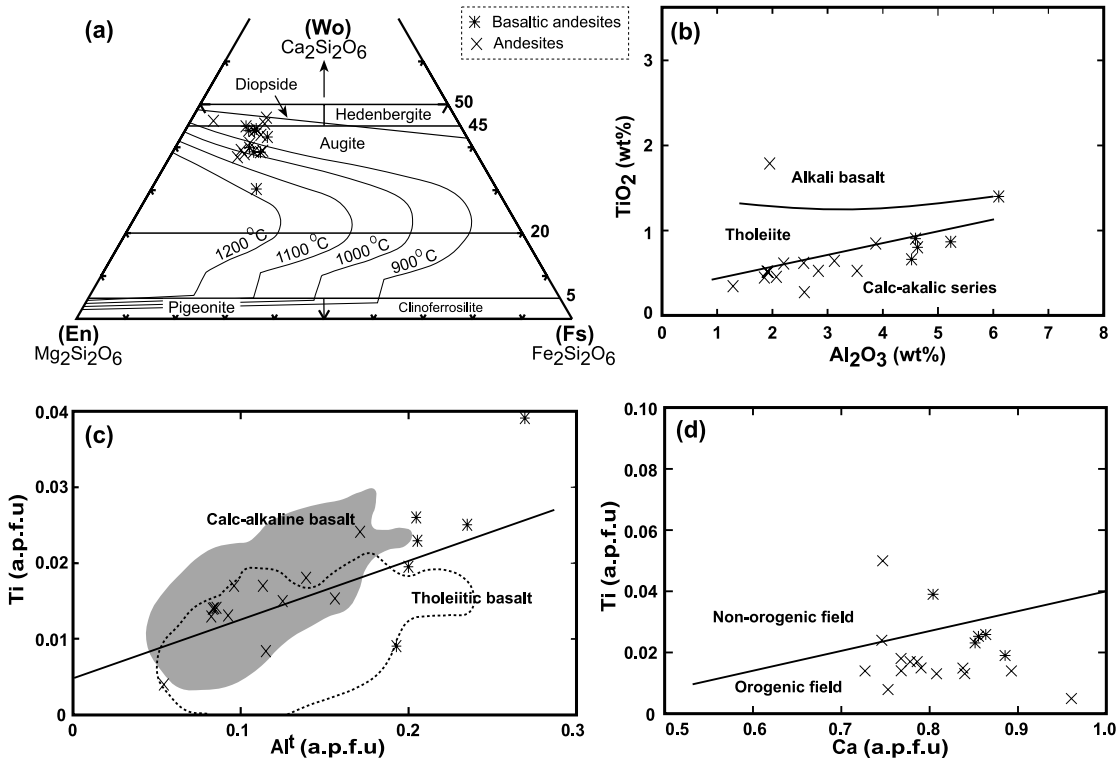

Figure 2. (a) Composition of clinopyroxenes from Wadi Hawashiya basaltic andesite and andesite dykes are depicted on the En–Wo–Fs clinopyroxene classification diagram after Morimoto (1988). (b) TiO_2 v. Al_2O_3 binary diagram after Le Bas (1962); (c) Ti v. total Al and (d) Ca v. Ti binary diagrams after Letterrier *et al*. (1982) modified by Sun & Bertrand (1991). a.p.f.u. – atoms per formula unit.

(1969), on glass discs (fusion beads) and pressed powder pellets, respectively. The analytical runs were calibrated using USGS and other international rock standards, and the analytical precision is better than 1 % and 3–5 % for major and trace elements, respectively. Microprobe analyses of silicate minerals were obtained using a fully automated Cameca Camebax CX-827 electron microprobe equipped with 3-spectrometers and a wavelength dispersive system. Natural materials were used as standards for microprobe analyses. The analyses were performed on polished thin-sections under operating conditions of accelerating voltage of about 15 kV and a beam current of about 30 nA.

6. Mineral chemistry

6.a. Clinopyroxene

The end-member composition for clinopyroxenes from basaltic andesites and andesites is $En_{38.0-62.5}Wo_{29.0-46.3}Fs_{4.8-21.4}$ (Table 1). The clinopyroxenes are mainly augite, but a few analyses from andesite plot in the diopside field of Morimoto (1988) (Fig. 2a). The clinopyroxenes from basaltic andesites and andesites reveal considerable variations in the concentrations of some oxides such as Al_2O_3 and CaO (see Table 1). The variations may be attributed to the original composition of the host rock, to variable degrees of alteration, or to disequilibrium states produced by fast rates of cooling (Löfgren, 1974). Na_2O contents are generally low, but slightly higher in clinopyroxenes from andesites. This low Na_2O content indicates low pressure of crystallization and the subalkaline nature of parental magma. On the Al_2O_3 v. TiO_2 binary diagram (Fig. 2b) of Le Bas (1962), the analysed clinopyroxenes fall in the calc-alkaline field with the exception of two points scattered in the other fields. Furthermore, on the total Al v. Ti plot (Fig. 2c), most clinopyroxenes fall in the calc-alkaline basalt field of Letterrier *et al*. (1982). Most clinopyroxenes lie in the orogenic field on the Ca–Ti discrimination diagram (Fig. 2d), consistent with formation in an arc-related tectonic setting. According to Lindsley (1983), the clinopyroxene composition yields the crystallization temperatures that range from 950 °C to ~1220 °C for basaltic andesites and from ~860 °C to ~1170 °C for andesites (Fig. 2a).

6.b. Amphibole

Amphiboles are calcic amphiboles according to Leake's (1978) classification, where $(Na+K)_B > 1.34$ and $Na_B < 0.67$ (Table 2). Overlapping variations in the contents of $(Na+K)_A$, Fe^{3+}, Al^{VI}, and Ti in amphiboles from basaltic andesites and andesites reveal two groups. The first group has $Si > 7$ apfu (atoms per formula unit), $(Na+K)_A < 0.5$ and are classified as

Table 2. Representative mineral chemistry of amphibole from Wadi Hawashiya dykes

Rock type	Basaltic andesites								Andesites													
Sample no.	221	221	200	200	242	242	224	224	243	243	257	257	281	281	234	234	268	268	235	235	254	254
Analysis	Hbl1-4	Hbl3-1	Hbl2-4	Hbl2-5	Hbl3-2	Hbl1-7	Hbl2-5	Hbl2-6	Hbl2-2	Hbl2-3	Hbl2-1	Hbl2-6	Hbl2-2	Hbl2-3	Hbl1-3	Hbl1-2	Hbl2-1	Hbl1-2	Hbl5-2	Hbl5-1	Hbl2-2	Hbl3-3
SiO_2	45.52	52.24	47.89	42.13	46.27	42.08	40.46	53.45	41.58	48.22	48.92	42.26	40.76	41.54	41.90	44.28	48.45	52.88	53.46	42.41	55.25	51.34
TiO_2	1.10	0.59	0.71	2.17	2.11	3.43	3.04	0.19	3.14	1.64	0.14	3.35	3.81	3.53	2.53	2.56	0.85	0.29	0.18	3.14	0.03	0.49
Al_2O_3	7.81	3.41	6.79	12.04	8.26	12.57	13.77	5.17	11.95	7.36	6.26	12.39	12.96	11.59	11.81	11.11	6.11	3.17	2.20	11.20	0.28	2.48
FeO	13.98	9.36	13.30	14.29	12.65	11.29	12.31	10.00	11.26	12.11	13.50	11.25	14.74	17.55	11.66	10.93	14.84	11.90	10.64	12.94	4.82	9.56
MnO	0.26	0.15	0.46	0.34	0.28	0.20	0.19	0.24	0.18	0.26	0.25	0.06	0.12	0.22	0.17	0.05	0.42	0.35	0.54	0.19	0.19	0.31
MgO	13.58	17.59	15.25	13.26	15.21	14.24	12.95	14.24	14.51	14.87	15.21	14.49	11.89	10.29	14.86	15.65	14.36	16.55	17.56	13.60	22.44	19.63
CaO	12.34	12.63	11.49	10.92	10.56	11.09	11.29	11.04	11.36	12.10	12.12	11.24	10.79	10.71	11.24	10.92	12.04	12.10	12.54	11.14	12.53	10.43
Na_2O	0.93	0.38	1.17	2.38	1.95	2.60	2.41	1.71	2.40	0.96	0.68	2.43	2.50	2.33	2.41	2.40	1.03	0.53	0.28	1.80	0.06	0.21
K_2O	0.49	0.14	0.34	0.59	0.36	0.42	0.49	0.11	0.46	0.33	0.25	0.52	0.56	0.77	0.53	0.48	0.49	0.19	0.00	0.52	0.03	0.96
Total	96.18	96.49	97.51	98.21	97.79	97.94	97.12	96.15	96.91	97.85	97.48	98.10	98.38	98.70	97.18	98.47	98.71	98.10	97.47	96.99	95.79	95.50
Numbers of cations on the basis of 23 oxygens																						
Si	6.757	7.489	6.921	6.153	6.692	6.117	5.974	7.840	6.105	6.949	7.054	6.131	6.014	6.197	6.121	6.344	6.997	7.534	7.602	6.234	7.736	7.348
Al^{iv}	1.243	0.511	1.079	1.847	1.305	1.883	2.026	0.160	1.895	1.051	0.946	1.869	1.986	1.803	1.879	1.656	1.001	0.466	0.368	1.766	0.046	0.418
Fe^{3+}	0.000	0.000	0.000	0.000	0.003	0.000	0.000	0.000	0.000	0.000	0.000	0.000	0.000	0.000	0.000	0.000	0.002	0.000	0.030	0.000	0.218	0.234
Sum T	8.000	8.000	8.000	8.000	8.000	8.000	8.000	8.000	8.000	8.000	8.000	8.000	8.000	8.000	8.000	8.000	8.000	8.000	8.000	8.000	8.000	8.000
Al^{vi}	0.122	0.065	0.077	0.224	0.102	0.269	0.368	0.733	0.172	0.198	0.117	0.247	0.266	0.233	0.153	0.218	0.038	0.065	0.000	0.173	0.000	0.000
Fe^{3+}	0.556	0.252	0.692	0.671	0.554	0.393	0.428	0.000	0.486	0.309	0.700	0.396	0.423	0.367	0.644	0.501	0.548	0.321	0.378	0.549	0.257	0.493
Ti	0.123	0.064	0.077	0.238	0.230	0.375	0.338	0.021	0.347	0.178	0.015	0.366	0.423	0.396	0.278	0.276	0.092	0.031	0.019	0.347	0.003	0.053
Mg	3.005	3.759	3.286	2.887	3.279	3.086	2.850	3.114	3.176	3.195	3.269	3.134	2.615	2.288	3.236	3.342	3.092	3.515	3.722	2.980	4.684	4.188
Fe^{2+}	1.178	0.851	0.840	0.958	0.819	0.864	1.004	1.117	0.808	1.105	0.884	0.854	1.266	1.702	0.678	0.660	1.205	1.046	0.848	0.939	0.045	0.248
Mn	0.016	0.009	0.028	0.021	0.017	0.012	0.012	0.015	0.011	0.016	0.015	0.004	0.007	0.014	0.010	0.003	0.026	0.021	0.032	0.012	0.011	0.019
Ca	0.000	0.000	0.000	0.000	0.000	0.000	0.000	0.000	0.000	0.000	0.000	0.000	0.000	0.000	0.000	0.000	0.000	0.000	0.000	0.000	0.000	0.000
Sum C	5.000	5.000	5.000	5.000	5.000	5.000	5.000	5.000	5.000	5.000	5.000	5.000	5.000	5.000	5.000	5.000	5.000	5.000	5.000	5.000	5.000	5.000
Mg	0.000	0.000	0.000	0.000	0.000	0.000	0.000	0.000	0.000	0.000	0.000	0.000	0.000	0.000	0.000	0.000	0.000	0.000	0.000	0.000	0.000	0.000
Fe^{2+}	0.001	0.019	0.075	0.115	0.154	0.115	0.088	0.109	0.088	0.046	0.044	0.115	0.130	0.121	0.102	0.149	0.038	0.050	0.009	0.103	0.045	0.170
Mn	0.016	0.009	0.028	0.021	0.017	0.012	0.012	0.015	0.011	0.016	0.015	0.004	0.008	0.014	0.011	0.003	0.026	0.021	0.033	0.012	0.011	0.019
Ca	1.962	1.940	1.779	1.709	1.636	1.727	1.786	1.735	1.787	1.868	1.872	1.747	1.708	1.712	1.759	1.676	1.863	1.847	1.910	1.755	1.880	1.599
Na	0.020	0.032	0.117	0.155	0.193	0.145	0.114	0.141	0.113	0.070	0.068	0.134	0.156	0.153	0.128	0.172	0.073	0.073	0.038	0.130	0.008	0.029
Sum B	2.000	2.000	2.000	2.000	2.000	2.000	2.000	2.000	2.000	2.000	2.000	2.000	2.000	2.000	2.000	2.000	2.000	1.991	1.991	2.000	1.944	1.817
Ca	0.000	0.000	0.000	0.000	0.000	0.000	0.000	0.000	0.000	0.000	0.000	0.000	0.000	0.000	0.000	0.000	0.000	0.000	0.000	0.000	0.000	0.000
Na	0.248	0.074	0.210	0.519	0.354	0.588	0.576	0.346	0.570	0.198	0.122	0.549	0.559	0.521	0.555	0.495	0.215	0.074	0.039	0.383	0.008	0.030
K	0.093	0.026	0.063	0.110	0.066	0.078	0.092	0.021	0.086	0.061	0.046	0.096	0.105	0.147	0.099	0.088	0.090	0.035	0.000	0.098	0.005	0.175
Sum A	0.340	0.099	0.273	0.629	0.421	0.666	0.668	0.366	0.656	0.259	0.168	0.645	0.665	0.668	0.654	0.583	0.306	0.108	0.039	0.480	0.014	0.205

Sum T – total of cations in the T – site; Sum C – total of cations in the C site; Sum B – sum of cations in B-site; Sum A – sum of cations in A-site.

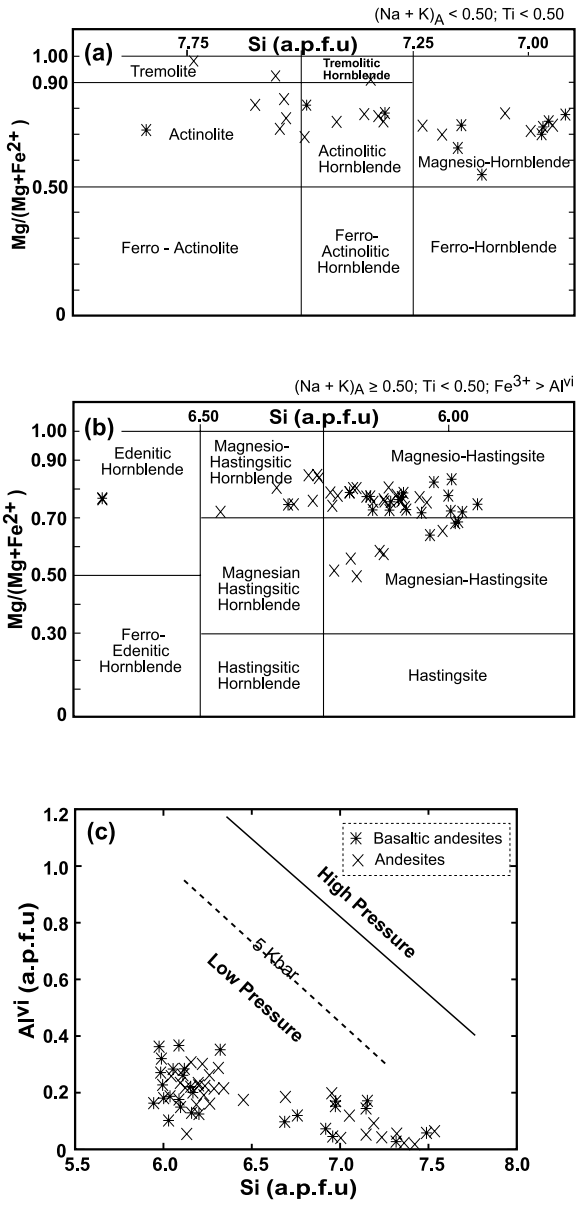

Figure 3. (a, b) Amphibole classification diagrams (Leake, 1978) for amphiboles in Hawashiya basaltic andesite and andesite dykes, and (c) Si v. Al^{vi} discrimination relation of amphibole as geobarometer index (Raase, 1974). a.p.f.u. – atoms per formula unit.

magnesio-hornblende, actinolitic hornblende, and actinolite as well as rarely tremolite (only two points) (Fig. 3a). The amphiboles of the other group have Si < 7 apfu, $(Na+K)_A > 0.5$ and are mainly magnesio-hastingsite, magnesian-hastingsite, and magnesio-hastingsitic hornblende with only two analyses in the edenitic hornblende field (Fig. 3b). The greater part of total Al occurs as Al^{IV}, reflecting the high temperature of crystallization. The analysed amphiboles fall in the low-pressure field on the Si and Al^{VI} diagram of Raase (1974) (Fig. 3c).

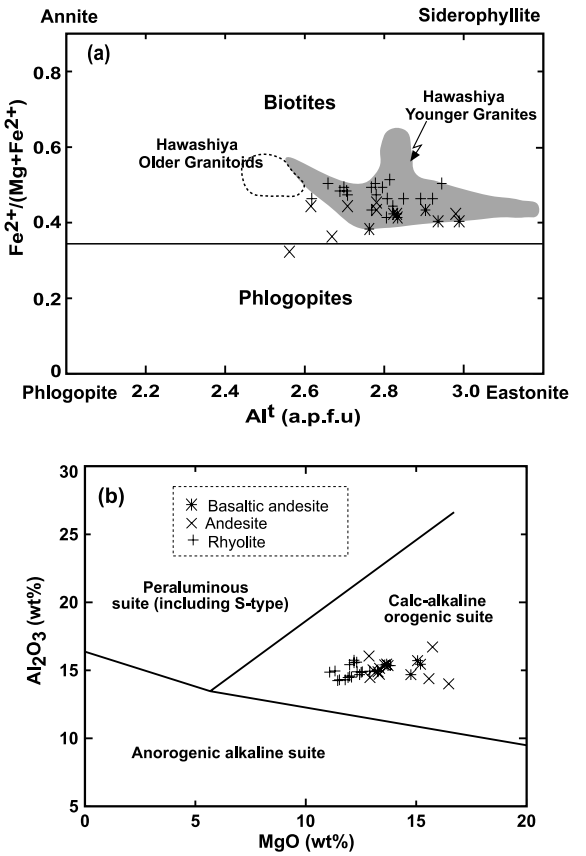

Figure 4. (a) Composition of biotites from Wadi Hawashiya dykes depicted graphically on the total Al v. $Fe^{2+}/(Mg + Fe^{2+})$ variation diagram; fields are from Eliwa, Dawoud & Negendank (1999). (b) MgO v. Al_2O_3 binary diagram (Abdel Rahman, 1994). a.p.f.u. – atoms per formula unit.

6.c. Biotite

The biotites (Table 3) plot in the biotite field on the Al^t v. $Fe^{2+}/(Fe^{2+} + Mg)$ discrimination diagram (Fig. 4a) of Deer, Howie & Zussman (1966). Ewart (1982) mentioned that the fields of biotites from orogenic basaltic andesites and andesites coincide with the fields of biotites from orogenic dacites and rhyolites. TiO_2 shows scattered and overlapping values in the basaltic andesites and andesites (1.92–4.64 wt %, av. 3.32 wt %) and (0.81–4.05 wt %, av. 2.73 wt %), respectively, which are relatively lower than that in rhyolites (3.51–4.65 wt %, av. 4.05 wt %). In the tetrahedral site, there is no coupled substitution between Al^{IV} and Ti, but on the other hand there is more substitution of Si by and Al^{IV}, which reflects a higher crystallization temperature of the biotites (Deer, Howie & Zussman, 1966). All analysed biotites fall within the field of calc-alkaline orogenic suite on the MgO v. Al_2O_3 discrimination diagram (Fig. 4b) of Abdel Rahman (1994).

6.d. Plagioclase

Plagioclase phenocrysts have a wide range of composition (Table 4), even within a single rock type as

Table 3. Representative mineral chemistry of biotite from Wadi Hawashiya dykes

Rock type	Basaltic andesites					Andesites						Rhyolites					
Sample no.	221	221	221	224	224	243	243	243	268	268	268	222	222	222	271	271	271
Analysis	Bt1-1	Bt1-2	Bt4-1	Bt1-4	Bt5-1	Bt3-1	Bt3-2	Bt5-1	Bt2-1	Bt5-1	Bt8-1	Bt4-1	Bt1-3	Bt2-1	Bt1-1	Bt1-3	Bt6-2
SiO_2	35.59	37.34	35.05	36.84	34.34	37.37	39.86	36.55	37.46	36.72	37.93	36.82	35.19	36.76	35.62	37.56	36.55
TiO_2	3.17	3.36	4.59	3.20	4.64	2.48	1.52	0.81	3.64	3.89	4.05	4.57	4.65	4.43	3.76	3.65	3.92
Al_2O_3	15.51	15.46	14.74	15.40	14.94	16.10	14.05	16.76	14.76	15.09	14.52	14.35	14.91	14.30	14.99	15.39	15.65
FeO	18.41	16.94	15.85	17.76	17.32	16.71	14.07	15.12	18.43	19.06	17.86	20.40	20.89	20.15	18.17	17.24	18.65
MnO	0.17	0.19	0.15	0.32	0.28	0.15	0.11	0.13	0.10	0.11	0.23	0.44	0.15	0.60	0.49	0.28	0.32
MgO	13.71	13.62	14.80	13.77	13.32	12.91	16.52	15.79	13.38	13.09	12.95	11.83	11.13	11.49	12.94	13.87	12.35
CaO	0.25	0.07	2.56	0.07	3.02	0.07	0.13	0.09	0.04	0.00	0.02	0.04	0.00	0.02	0.09	0.04	0.00
BaO	0.15	0.35	0.04	0.16	0.04	0.31	0.00	0.24	0.05	0.00	0.00	0.07	0.79	0.49	0.02	0.00	0.00
Na_2O	0.09	0.12	0.14	0.10	0.04	0.11	0.12	0.12	0.17	0.08	0.12	0.10	0.09	0.10	0.14	0.36	0.13
K_2O	7.88	9.22	5.10	9.04	5.53	9.23	8.03	7.97	8.82	8.70	8.60	8.25	8.40	8.69	8.61	8.14	8.90
Rb_2O	0.15	0.12	0.13	0.17	0.15	0.17	0.22	0.13	0.21	0.22	0.18	0.16	0.17	0.19	0.17	0.25	0.19
Total	95.18	96.95	93.20	96.98	93.77	93.90	95.77	93.79	97.11	97.18	96.75	97.69	96.16	97.66	95.17	96.92	96.81
F^-	0.07	0.04	0.12	0.22	0.32	0.10	0.11	0.00	0.14	0.16	0.17	0.69	0.84	0.69	0.82	0.63	0.37
Numbers of cations on the basis of 24 oxygens																	
Si	5.653	5.806	5.573	5.749	5.505	5.868	6.165	5.772	5.830	5.739	5.907	5.699	5.633	5.798	5.688	5.808	5.728
Al^{IV}	2.347	2.194	2.427	2.251	2.495	2.132	1.835	2.228	2.170	2.261	2.093	2.301	2.367	2.202	2.312	2.192	2.272
Tetrahedral (Z)	8.000	8.000	8.000	8.000	8.000	8.000	8.000	8.000	8.000	8.000	8.000	8.000	8.000	8.000	8.000	8.000	8.000
Al^{VI}	0.554	0.637	0.333	0.579	0.325	0.845	0.724	0.889	0.535	0.517	0.570	0.314	0.444	0.454	0.507	0.611	0.617
Ti	0.379	0.393	0.549	0.376	0.560	0.293	0.177	0.096	0.426	0.457	0.474	0.532	0.560	0.526	0.452	0.425	0.462
Fe^{2+}	2.446	2.203	2.107	2.318	2.322	2.194	1.820	1.997	2.399	2.491	2.326	2.640	2.797	2.658	2.426	2.229	2.444
Mn	0.023	0.025	0.020	0.042	0.038	0.020	0.014	0.017	0.013	0.015	0.030	0.058	0.020	0.080	0.066	0.037	0.042
Mg	3.247	3.157	3.508	3.204	3.183	3.022	3.809	3.717	3.104	3.050	3.007	3.073	2.656	2.702	3.080	3.197	2.885
Octahedral (Y)	6.649	6.415	6.517	6.519	6.428	6.374	6.544	6.716	6.477	6.530	6.407	6.617	6.477	6.420	6.531	6.499	6.450
Ca	0.043	0.012	0.436	0.012	0.519	0.012	0.022	0.015	0.007	0.000	0.003	0.007	0.000	0.003	0.015	0.007	0.000
Ba	0.010	0.020	0.000	0.010	0.000	0.020	0.000	0.010	0.000	0.000	0.000	0.000	0.050	0.030	0.000	0.000	0.000
Na	0.028	0.036	0.043	0.030	0.012	0.033	0.036	0.037	0.051	0.024	0.036	0.030	0.028	0.031	0.043	0.108	0.040
K	1.597	1.829	1.034	1.800	1.131	1.849	1.584	1.606	1.751	1.735	1.709	1.629	1.715	1.749	1.754	1.606	1.779
Interlayer (X)	1.678	1.897	1.513	1.852	1.662	1.914	1.642	1.668	1.809	1.759	1.748	1.666	1.793	1.813	1.812	1.721	1.819

Table 4. Representative mineral chemistry of plagioclase from Wadi Hawashiya dykes

Rock type	Basaltic andesites								Andesites											Rhyolites				
Sample no.	212	212	242	242	200	200	224	224	243	243	257	254	254	281	234	234	234	268	268	222	222	222	271	271
Analysis	P2-2	P3-1	P6-1	P5-1	P6-1	P8-1	P1-1	P1-3	P1-1	P7-1	P2-1	P7-5	P7-7	P2-1	P1-1	P1-4	P2-1	P4-3	P9-2	P3-2	P3-3	P3-5	P3-1	P5-1
SiO_2	60.31	64.45	64.88	54.67	57.35	64.37	53.01	62.87	54.51	64.76	64.29	53.26	52.36	64.71	63.01	59.66	55.28	53.02	61.06	61.94	61.35	63.05	62.19	63.48
TiO_2	0.05	0.01	0.01	0.00	0.00	0.03	0.05	0.00	0.01	0.22	0.00	0.08	0.13	0.00	0.04	0.02	0.04	0.00	0.01	0.00	0.00	0.00	0.02	0.00
Al_2O_3	23.97	21.23	21.91	28.06	27.48	22.20	29.18	23.23	28.07	21.59	21.21	29.55	30.28	22.27	22.33	25.22	27.76	30.14	24.26	23.68	24.57	23.46	23.50	23.36
MgO	0.23	0.02	0.01	0.01	0.01	0.01	0.02	0.04	0.00	0.00	0.00	0.46	0.37	0.00	0.08	0.00	0.02	0.00	0.00	0.00	0.00	0.00	0.00	0.00
CaO	5.17	1.74	1.53	10.26	7.09	2.76	10.96	2.78	9.93	1.89	2.11	2.96	3.88	2.91	2.98	6.24	9.66	11.97	5.43	4.73	5.16	3.79	3.87	3.40
MnO	0.02	0.02	0.02	0.00	0.00	0.01	0.00	0.07	0.00	0.00	0.00	0.10	0.01	0.00	0.00	0.04	0.07	0.02	0.02	0.00	0.02	0.01	0.00	0.02
FeO	0.57	0.23	0.13	0.33	0.13	0.18	0.49	0.04	0.41	0.24	0.08	1.64	1.20	0.06	0.06	0.01	0.54	0.18	0.28	0.17	0.08	0.12	0.23	0.00
Rb_2O	0.27	0.23	0.25	0.22	0.26	0.27	0.24	0.28	0.20	0.28	0.25	0.22	0.24	0.24	0.30	0.25	0.26	0.19	0.23	0.20	0.22	0.27	0.30	0.24
Na_2O	7.28	8.80	10.99	6.02	6.67	9.72	5.10	9.23	5.81	10.23	9.65	3.58	3.78	9.74	9.95	7.74	6.07	4.90	8.56	9.13	8.90	9.07	8.83	9.28
K_2O	1.82	2.72	0.10	0.21	0.89	0.13	0.17	0.71	0.26	0.52	1.19	6.44	5.52	0.15	0.43	0.38	0.14	0.11	0.33	0.20	0.22	0.49	0.33	0.27
Cs_2O	0.07	0.00	0.05	0.12	0.16	0.00	0.05	0.00	0.00	0.07	0.04	0.00	0.00	0.05	0.00	0.00	0.04	0.01	0.05	0.08	0.00	0.09	0.12	0.00
BaO	0.13	0.05	0.09	0.00	0.05	0.08	0.01	0.00	0.01	0.34	0.18	0.05	0.30	0.05	0.01	0.00	0.07	0.00	0.03	0.10	0.07	0.10	0.04	0.00
Total	99.89	99.50	99.97	99.90	100.09	99.76	99.28	99.25	99.21	100.14	99.00	98.34	98.07	100.18	99.19	99.56	99.95	100.54	100.26	100.23	100.59	100.45	99.43	100.05
Numbers of cations on the basis of 32 oxygens																								
Si	10.853	11.527	11.462	9.923	10.300	11.393	9.692	11.212	9.938	11.466	11.514	9.916	9.767	11.402	11.268	10.696	10.012	9.574	10.873	11.008	10.869	11.147	11.105	11.213
Ti	0.007	0.001	0.001	0.000	0.000	0.004	0.007	0.000	0.001	0.029	0.000	0.011	0.018	0.000	0.005	0.003	0.005	0.000	0.001	0.000	0.000	0.000	0.003	0.000
Al	5.084	4.476	4.562	6.003	5.817	4.632	6.289	4.883	6.032	4.506	4.477	6.485	6.657	4.625	4.707	5.329	5.926	6.415	5.092	4.960	5.131	4.889	4.946	4.863
Mg	0.062	0.005	0.003	0.003	0.003	0.003	0.005	0.011	0.000	0.000	0.000	0.128	0.103	0.000	0.021	0.000	0.005	0.000	0.000	0.000	0.000	0.000	0.000	0.000
Ca	0.997	0.333	0.290	1.995	1.364	0.523	2.147	0.531	1.940	0.359	0.405	0.591	0.775	0.549	0.571	1.199	1.875	2.316	1.036	0.901	0.980	0.718	0.740	0.643
Mn	0.003	0.003	0.003	0.000	0.000	0.001	0.000	0.011	0.000	0.000	0.000	0.016	0.002	0.000	0.000	0.006	0.011	0.003	0.003	0.000	0.003	0.001	0.000	0.003
Fe^{2+}	0.086	0.034	0.019	0.050	0.020	0.027	0.075	0.006	0.063	0.036	0.012	0.255	0.187	0.009	0.009	0.001	0.082	0.027	0.042	0.025	0.012	0.018	0.034	0.000
Rb	0.031	0.026	0.028	0.026	0.030	0.031	0.028	0.032	0.023	0.032	0.029	0.026	0.029	0.027	0.034	0.029	0.030	0.022	0.026	0.023	0.025	0.031	0.034	0.027
Na	2.540	3.052	3.764	2.119	2.323	3.336	1.808	3.192	2.054	3.512	3.351	1.292	1.367	3.328	3.450	2.690	2.132	1.716	2.956	3.146	3.057	3.109	3.057	3.178
K	0.418	0.621	0.023	0.049	0.204	0.029	0.040	0.162	0.060	0.117	0.272	1.530	1.314	0.034	0.098	0.087	0.032	0.025	0.075	0.045	0.050	0.111	0.075	0.061
Cs	0.005	0.000	0.004	0.009	0.012	0.000	0.004	0.000	0.000	0.005	0.003	0.000	0.000	0.004	0.000	0.000	0.003	0.001	0.004	0.006	0.000	0.007	0.009	0.000
Ba	0.009	0.004	0.006	0.000	0.004	0.006	0.001	0.000	0.001	0.024	0.013	0.004	0.022	0.003	0.001	0.000	0.005	0.000	0.002	0.007	0.005	0.007	0.003	0.000
Total cations	20.10	20.08	20.17	20.18	20.08	19.98	20.10	20.04	20.11	20.09	20.08	20.25	20.24	19.98	20.16	20.04	20.12	20.10	20.11	20.12	20.13	20.04	20.01	19.99
Ab	64.23	76.18	92.34	50.90	59.51	85.78	45.26	82.16	50.66	88.06	83.20	37.87	39.55	85.09	83.76	67.67	52.78	42.29	72.68	76.88	74.81	78.96	78.94	81.86
An	25.21	8.32	7.10	47.94	34.96	13.46	53.75	13.68	47.85	8.99	10.05	17.30	22.44	14.05	13.86	30.15	46.42	57.09	25.48	22.01	23.97	18.23	19.12	16.57
Or	10.57	15.49	0.55	1.17	5.22	0.75	0.99	4.16	1.49	2.95	6.75	44.83	38.01	0.86	2.38	2.19	0.80	0.62	1.84	1.11	1.22	2.81	1.94	1.57

Ab – albite; An – anorthite; Or – orthoclase.

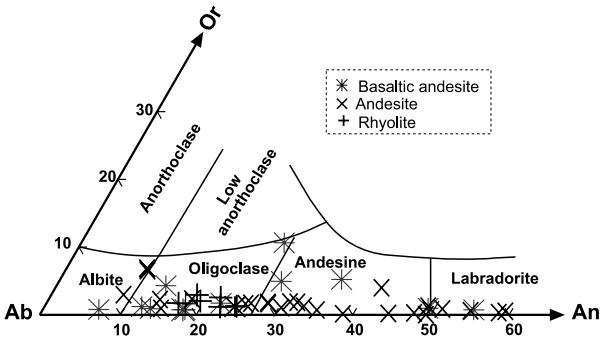

Figure 5. Ternary Ab–Or–An classification diagram of feldspars (Deer, Howie & Zussmann, 1966).

elucidated on the Ab–Or–An ternary diagram (Fig. 5). Plagioclase is labradorite to oligoclase in basaltic andesites ($An_{53.7-12.2}$) and labradorite to albite in andesites ($An_{57.3-8.2}$), whereas it is oligoclase ($An_{24.0-13.4}$) in dacites. This wide range of plagioclase compositions in the mafic dyke suite is attributed to variable degrees of saussuritization.

7. Whole rock geochemistry

7.a. Major and trace element geochemistry

Chemical analyses of 27 representative samples of Wadi Hawashiya dykes are given in Table 5. The chemical variations among the different dykes are best presented on the Harker variation diagrams (Fig. 6). The histogram shows the distribution of SiO_2 between the mafic and felsic dyke suites (a small SiO_2 gap, 3.5 wt %) compared to other dyke suites from the north Eastern Desert and Sinai (Fig. 7). As a whole, CaO, MnO, TiO_2 and Fe_2O_3 show negative correlation, whereas MgO and P_2O_5 show somewhat negative correlation with increasing SiO_2. Na_2O and K_2O increase irregularly with increasing SiO_2. The MgO content of most mafic dyke samples varies between 5.18 wt % and 8.96 wt % with four samples having less than 4 wt %, while that of the felsic dyke suite is very low (0.18–0.80 wt %) (Table 5). Mg numbers (molar 100 $Mg/Mg + Fe^{2+}$) in the mafic dykes are 18–76, while in the felsic dykes they are 13–41. On the basis of MgO content in the mafic dyke suite at nearly constant SiO_2, two populations of andesites can be recognized: high MgO andesites (MgO > 4 wt %, Mg number > 57) and low MgO andesites (MgO < 4 wt %, Mg number < 54). This feature has been previously observed in the host Hawashiya older granitoids (Eliwa, Dawoud & Negendank, 1999). The mafic dyke suite is characterized by moderate Al_2O_3 (13.52–17.89 wt %) and low TiO_2 (0.73–1.28 wt %) and CaO (3.64–7.85) contents, the felsic dyke suite has moderate contents of CaO (0.30–2.20 wt %). The mafic dyke suite is characterized by greater abundances of Cr, V and Ni (131–250 ppm, 60–158 ppm, 7–141 ppm) relative to the felsic dyke suite (0–2 ppm, 13–23 ppm, 7–8 ppm), respectively. Rb, Y, Zr and La do not exhibit systematic variation in the mafic dykes, but decrease in the felsic dykes with increasing SiO_2. Nb and Sr increase in the mafic dykes but decrease in the felsic dykes with increasing SiO_2. In both the mafic and felsic dykes, Ba increases with increasing SiO_2.

7.b. Magma type

On the various classification diagrams using the mobile elements $Na_2O + K_2O$ v. SiO_2 of Le Maitre (1989) (Fig. 8a), and immobile elements Zr/TiO_2 v. SiO_2 of Winchester & Floyd (1977) (Fig. 8b), the Hawashiya dykes are classified as subalkaline basaltic andesites, andesites, dacites and rhyolites as well as trachy-andesites. The dykes range from medium-K (mafic dykes) to high-K calc-alkaline series (felsic dykes) (Fig. 6). On the Alk–FeO*–MgO diagram (Fig. 9a) of Irvine & Baragar (1971), and on the FeO*/MgO v. SiO_2 diagram (Fig. 9b) of Miyashiro (1974), the dykes are typically of calc-alkaline nature (except sample no. 257 is tholeiite). This is in accordance with the calc-alkaline affinity obtained from the analysed clinopyroxene and biotite phenocrysts.

The magma type(s) of the mafic volcanic dykes and their source can be further distinguished on the basis of the Th/Yb v. Ta/Yb discriminant diagram (Fig. 9c) of Pearce (1982). This diagram utilizes the Ta/Yb ratio to distinguish subduction components from normal mantle-derived melt compositions, while the Th/Yb serves as a measure of the enrichment of the highly to less incompatible HFS elements. This diagram confirms the calc-alkaline character of the mafic dykes, which plot in and straddle the upper boundary of active continental margin field (except one sample lies in the oceanic island arc field).

7.c. Spider diagrams

Multi-element-normalized (spider) diagrams of Wadi Hawashiya dykes and other dyke and rock suites from different localities in the Eastern Desert and Sinai are shown in Figure 10a, b. Hawashiya dykes exhibit an overall enrichment relative to the normalizing values of Thompson, Hendry & Parry (1984). Both the mafic and felsic dyke suite patterns show LILE (Rb and K) enrichment and deep Nb–Ta troughs. A significant negative Nb–Ta anomaly may be due to retention of Nb and Ta within a stable mineral phase (titanite?zircon?: Pearce, 1983; amphiboles?: Hofmann, 1988) in the source region. Nb depletion is typical of all island arc volcanic rocks (Hofmann, 1988) as well as calc-alkaline rocks from other destructive plate margins such as continental margins (Pearce, 1983; Thompson, Hendry & Parry, 1984), but also found in many continental within-plate basalts (Duncan, 1987). The felsic dyke suite shows further distinct negative Sr, P and Ti anomalies which

Table 5. Chemical composition of Wadi Hawashiya dykes

Rock type	Basaltic andesites										Andesites											Dacites		Rhyolites			
Sample no.	212	245	242	221	239	259	250	200	251	224	254	243	276	268	226	203	248	235	257	234	281	214	274	222	208	271	210
SiO_2	52.26	52.89	53.69	54.15	54.82	54.99	55.12	56.10	56.50	56.51	57.40	57.77	57.98	58.10	58.15	58.45	58.49	58.64	59.21	60.50	62.49	65.91	68.80	70.83	72.03	72.53	75.17
TiO_2	0.88	1.16	1.12	1.17	0.98	1.03	0.93	1.23	1.20	1.06	0.95	0.59	0.91	0.9	1.07	0.91	0.88	0.91	1.28	0.79	0.73	0.41	0.31	0.38	0.13	0.2	0.12
Al_2O_3	15.64	14.55	14.09	13.95	14.14	14.86	14.43	15.37	14.69	14.43	15.55	14.52	17.89	14.63	15.00	15.76	13.93	13.98	13.52	14.06	15.64	15.00	14.05	14.94	13.07	14.59	13.65
Fe_2O_3	9.52	9.36	8.83	8.69	8.20	8.31	8.37	8.58	7.59	7.81	7.61	5.43	6.12	7.29	7.12	7.71	6.71	6.82	9.94	6.08	6.6	5.07	4.11	2.32	1.46	1.09	0.84
MnO	0.15	0.17	0.14	0.14	0.15	0.13	0.17	0.13	0.13	0.13	0.12	0.09	0.12	0.12	0.11	0.14	0.11	0.11	0.19	0.11	0.11	0.09	0.09	0.05	0.03	0.03	0.03
MgO	8.06	8.18	8.96	8.47	8.54	7.56	8.35	5.84	6.63	7.01	5.18	8.56	3.61	6.41	\5.81	1.83	7.22	7.02	1.11	6.28	2.11	0.52	0.30	0.80	0.18	0.38	0.19
CaO	7.24	6.62	5.61	6.80	6.34	6.19	5.90	5.97	6.37	5.8	6.13	3.04	6.16	5.6	5.27	4.11	5.19	5.32	7.85	4.91	3.64	2.20	1.73	1.37	0.30	1.60	0.54
Na_2O	2.85	3.20	3.64	3.29	3.41	3.59	3.45	3.66	3.59	3.96	4.04	3.24	4.91	3.62	3.99	4.30	3.97	3.31	3.41	3.65	4.20	4.88	5.04	4.38	5.20	4.84	3.92
K_2O	1.60	1.21	1.80	1.61	1.20	1.29	1.45	1.84	1.80	1.21	1.41	2.38	1.17	2.39	1.99	3.20	2.17	2.20	1.60	2.14	2.82	3.80	3.96	3.87	3.68	4.29	5.17
P_2O_5	0.23	0.35	0.31	0.09	0.30	0.30	0.30	0.38	0.47	0.33	0.30	0.26	0.26	0.30	0.32	0.41	0.24	0.24	0.37	0.22	0.29	0.10	0.05	0.15	0.01	0.07	0.02
LOI	1.56	2.32	1.81	1.45	1.93	1.76	1.53	0.91	1.03	1.75	1.30	3.13	0.87	0.64	1.17	3.19	1.09	1.45	1.52	1.24	1.37	2.02	1.56	0.92	3.90	0.37	0.35
Total	99.99	100.01	100.00	99.81	100.01	100.01	100.00	100.01	100.00	100.00	99.99	99.01	100.00	100.00	100.00	100.01	100.00	100.00	100.00	99.98	100.00	100.00	100.00	100.01	99.99	99.99	100.00
Mg no.	62.64	63.38	66.77	65.87	67.35	64.31	66.39	57.41	63.37	64.00	57.41	75.54	53.88	63.52	61.77	31.98	68.06	67.09	18.11	67.17	38.77	16.88	12.63	40.58	19.62	40.84	30.94
Trace elements (ppm)																											
Rb	50	37	46	44	37	38	51	40	44	30	36	75	45	79	42	71	52	51	36	56	78	115	111	106	93	73	72
Sr	608	657	599	666	657	733	676	680	779	660	741	427	705	546	703	434	723	726	686	671	466	272	225	333	99	723	151
Y	20	18	17	20	20	21	19	17	21	19	19	32	18	19	17	34	14	14	22	18	38	36	42	15	35	9	10
Zn	98	–	–	–	83	–	107	–	99	–	88	90	–	74	88	93	–	–	–	85	95	98	–	42	153	21	–
Ni	125	–	–	–	141	–	123	–	122	–	28	7	–	77	78	7	–	–	–	117	8	7	–	8	8	7	–
Pb	5	–	–	–	6	–	8	–	7	–	15	18	–	13	12	14	–	–	–	8	21	23	–	19	13	25	–
Ga	12	15	–	–	–	–	–	13	–	–	20	–	–	17	–	–	–	–	–	–	14	20	–	19	–	18	–
V	154	138	–	–	–	–		142	–	–	158	–	–	134	–	–	–	–	–	–	60	–	–	23	–	13	–
Cr	144	250	–	–	–	–	–	131	–	–	123	–	–	202	–	–	–	–	–	–	–	2	–	–	–	–	–
Co	24	20	–	–	–	–	–	13	–	–	23	–	–	22	–	–	–	–	–	–	4	2	–	3	–	2	–
Zr	98	145	103	125	123	126	121	124	138	128	122	212	119	135	131	289	142	143	154	112	225	315	384	193	232	100	92
Nb	1.8	4	–	–	–	–	–	4.8	–	–	4.2	–	–	4.4	–	–	–	–	–	–	5.5	11.3	–	6	–	2.9	–
Cs	6.5	4.4	–	–	–	–	–	4.1	–	–	5.8	–	–	6.7	–	–	–	–	–	–	3.4	2.1	–	2.7	–	1.6	–
Ba	473	561	–	–	–	–	–	545	–	–	630	–	–	486	–	–	–	–	–	–	769	1003	–	1160	–	1190	–
Hf	2.7	3.7	–	–	–	–	–	3.6	–	–	3.8	–	–	3.9	–	–	–	–	–	–	5.8	8.1	–	5.1	–	3.6	–
Ta	0.28	0.35	–	–	–	–	–	0.5	–	–	0.34	–	–	0.48	–	–	–	–	–	–	0.6	0.9	–	0.68	–	0.34	–
Th	2.68	2.85	–	–	–	–	–	2.93	–	–	3.5	–	–	5.95	–	–	–	–	–	–	8.61	12.7	–	11.5	–	5.24	–
U	0.89	1.65	–	–	–	–	–	1.02	–	–	1.29	–	–	2.48	–	–	–	–	–	–	2.99	4.69	–	4	–	1.73	–
REE (ppm)																											
La	14.90	36.30	–	–	–	–	–	19.00	–	–	18.50	–	–	18.50	–	–	–	–	–	–	30.80	32.00	–	27.00	–	18.60	–
Ce	32.70	76.70	–	–	–	–	–	41.90	–	–	39.70	–	–	40.30	–	–	–	–	–	–	65.10	62.70	–	57.00	–	36.40	–
Pr	4.15	9.12	–	–	–	–	–	5.45	–	–	5.13	–	–	5.09	–	–	–	–	–	–	7.89	7.12	–	5.92	–	3.95	–
Nd	18.30	37.20	–	–	–	–	–	24.30	–	–	22.30	–	–	21.80	–	–	–	–	–	–	33.30	30.20	–	22.00	–	14.50	–
Sm	3.99	7.62	–	–	–	–	–	5.12	–	–	4.52	–	–	4.42	–	–	–	–	–	–	6.97	5.62	–	4.02	–	2.29	–
Eu	1.29	1.82	–	–	–	–	–	1.59	–	–	1.37	–	–	1.20	–	–	–	–	–	–	1.49	1.22	–	0.92	–	0.62	–
Gd	3.67	6.34	–	–	–	–	–	4.44	–	–	3.89	–	–	3.86	–	–	–	–	–	–	6.08	4.34	–	2.95	–	1.46	–
Tb	0.6	1.10	–	–	–	–	–	0.71	–	–	0.61	–	–	0.61	–	–	–	–	–	–	1.06	0.71	–	0.44	–	0.21	–
Dy	3.31	6.04	–	–	–	–	–	3.53	–	–	3.15	–	–	3.14	–	–	–	–	–	–	6.00	4.04	–	2.18	–	1.07	–
Ho	0.66	1.17	–	–	–	–	–	0.63	–	–	0.62	–	–	0.63	–	–	–	–	–	–	1.17	0.67	–	0.41	–	0.21	–
Er	1.99	3.41	–	–	–	–	–	1.65	–	–	1.80	–	–	1.88	–	–	–	–	–	–	3.51	1.81	–	1.22	–	0.71	–
Tm	0.28	0.52	–	–	–	–	–	0.21	–	–	0.25	–	–	0.26	–	–	–	–	–	–	0.53	0.26	–	0.17	–	0.11	–
Yb	1.75	3.38	–	–	–	–	–	1.22	–	–	1.60	–	–	1.70	–	–	–	–	–	–	3.38	1.48	–	1.17	–	0.77	–
Lu	0.28	0.48	–	–	–	–	–	0.16	–	–	0.24	–	–	0.25	–	–	–	–	–	–	0.49	0.28	–	0.18	–	0.13	–
CIPW Norm																											
Q	4.60	6.07	3.02	5.00	6.97	7.17	6.86	8.78	8.58	8.69	10.20	11.19	8.23	9.09	9.70	11.50	8.06	11.45	20.00	13.32	17.19	18.20	21.17	26.65	26.77	24.48	31.15
Or	9.48	7.17	10.66	9.53	7.11	7.64	8.59	10.89	10.66	7.16	8.35	14.10	6.93	14.16	11.78	18.94	12.85	13.02	9.47	12.67	16.70	22.50	23.45	22.91	21.79	25.38	30.38
Ab	24.11	27.07	30.30	27.84	28.85	30.37	29.19	30.97	30.37	33.51	34.18	27.41	41.54	30.63	33.76	36.38	33.59	28.01	28.85	30.88	35.54	41.29	42.64	37.06	44.00	40.95	33.17
An	25.20	21.81	16.81	18.56	19.75	20.65	19.63	20.12	18.67	18.05	20.19	13.54	23.35	16.64	17.16	14.26	13.80	16.81	16.87	15.68	15.55	7.85	4.01	6.24	1.45	5.49	2.60
Di	5.55	4.44	4.57	8.81	5.62	4.12	4.22	2.80	5.08	4.38	4.58	0.00	2.39	5.33	3.03	0.77	6.24	4.32	5.97	4.07	0.00	1.33	1.61	0.00	0.00	1.56	0.00
Hy	17.51	18.32	20.20	17.02	18.66	16.92	18.84	13.25	14.16	15.43	10.78	21.32	7.88	13.50	13.07	4.20	15.09	15.49	0.00	13.76	5.25	0.68	0.00	1.99	0.45	0.24	0.47
Hm	9.52	9.36	8.83	8.69	8.2.0	8.31	8.37	8.58	7.59	7.81	7.61	5.43	6.12	7.29	7.12	7.71	6.71	6.82	9.94	6.08	6.6.0	5.07	4.11	2.32	1.46	1.09	0.84
Il	0.34	0.33	0.3.0	0.30	0.36	0.28	0.39	0.26	0.31	0.28	0.27	0.19	0.26	0.25	0.25	0.30	0.23	0.23	0.40	0.26	0.24	0.19	0.19	0.11	0.07	0.07	0.06
Tn	1.73	2.42	2.37	2.49	1.95	2.17	1.77	2.69	2.55	2.25	1.99	0.00	1.90	1.89	2.30	1.85	1.86	1.93	2.62	1.60	0.70	0.76	0.51	0.00	0.01	0.41	0.00
Ap	0.55	0.83	0.74	0.21	0.71	0.71	0.71	0.91	1.12	0.78	0.72	0.62	0.62	0.72	0.76	0.97	0.57	0.57	0.88	0.52	0.70	0.24	0.12	0.37	0.02	0.17	0.05

LOI – Loss On Ignition; Q – Quartz; Or – Orthoclase; Ab – Albite; An – Anorthite; Di – Diopside; Hy – Hypersthene; Hm – Hematite; Il – Ilmenite; Tn – Titanite.

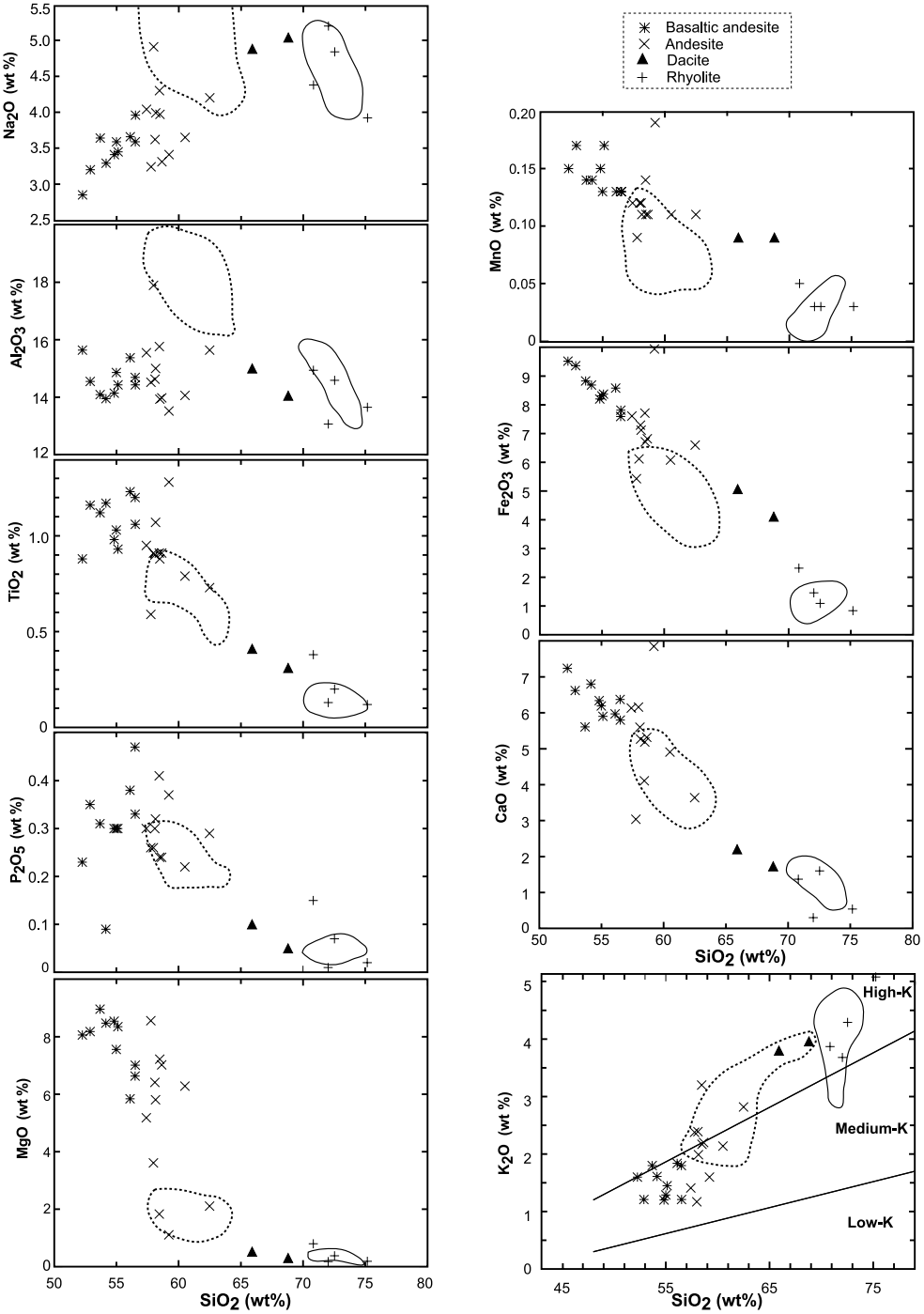

Figure 6. Harker variation diagrams for Wadi Hawashiya dykes. Fields delineated by dashed and solid lines represent the Hawashiya older granitoids and younger granites, respectively.

might reflect either fractionation of feldspar, apatite and titanite from melt, respectively, or retention of these minerals in the magma source within the crust. The enrichment of LREE and LILE relative to Nb and Ta is considered to reflect either crustal contamination (Wilson, 1989; Hofmann & Stein, 1994) and/or production of mafic magmas in a mantle that has been enriched in LILE and LREE by fluids from a subducted plate (Gill, 1981; Pearce, 1983; Condie, 1990).

7.d. Rare earth element patterns

Chondrite-normalized REE patterns for Wadi Hawashiya dykes (Fig. 11a, b) display moderate to relatively strong enrichment in the light rare earth elements (LREE) ($La_N = 40–99$) with La abundances of ~60–170 times chondritic values (Evenesen, Hamilton & O'Nions, 1978). REE patterns for the mafic dyke suite are moderately fractionated with

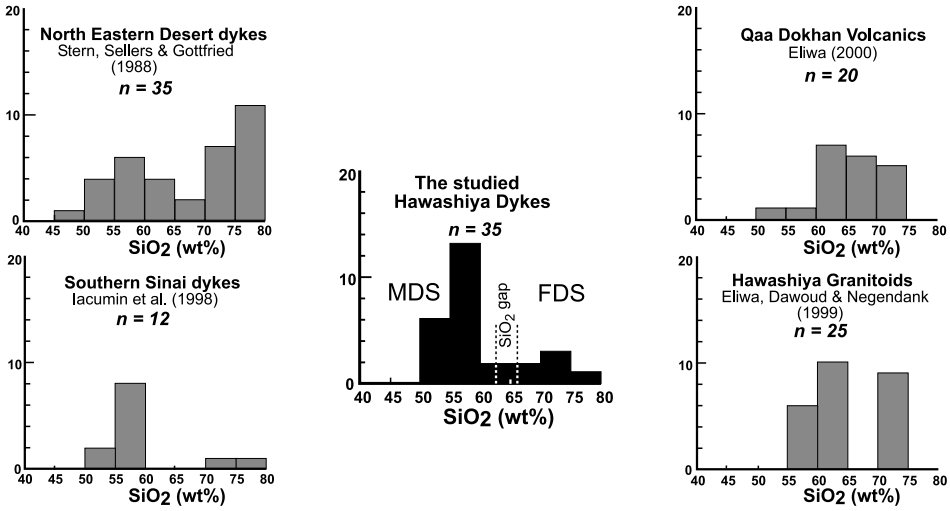

Figure 7. Histograms showing distribution of SiO_2 (wt %) in Hawashiya dyke suites, associated rocks and other dyke suites. MDS – mafic dyke suite, FDS – felsic dyke suite.

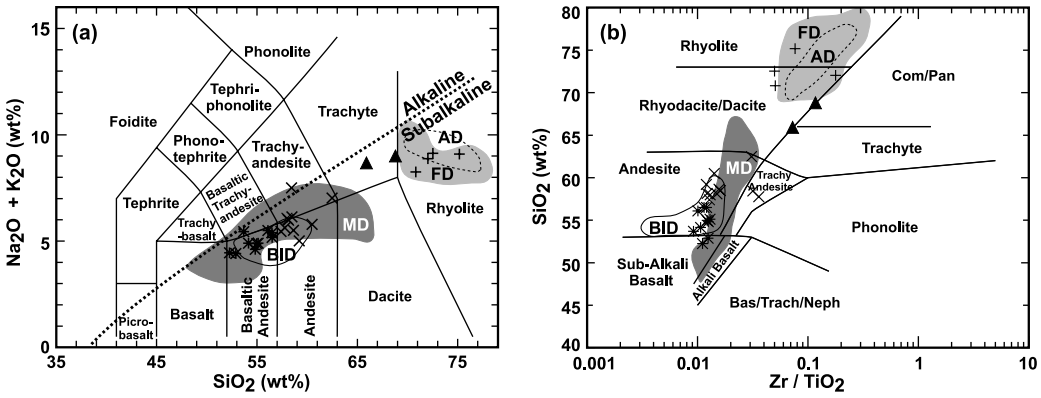

Figure 8. Geochemical classification of Wadi Hawashiya dyke using (a) TAS diagram (Le Maitre, 1989) and (b) Zr/TiO_2 v. SiO_2 diagram (Winchester & Floyd, 1977). Compared fields of mafic (MD) and felsic (FD) dykes from the north Eastern Desert (Stern, Sellers & Gottfried, 1988) and of basic-intermediate (BID) and acidic (AD) dykes from Southern Sinai (Iacumin *et al*. 1998). Com – comendite, Pan – pantellerite, Bas – basanite, Trach – trachybasalt, Neph – nephelinite. Symbols as in Figure 6.

$(La/Yb)_N = 5.75–10.52$ (av. 7.5), while those for the felsic dyke suite are strongly fractionated with $(La/Yb)_N = 14.6–16.32$ (av. 15.51). The HREE contents are more depleted in the felsic relative to those in the mafic dyke suite.

8. Discussion

8.a. Tectonic setting

Various investigators have used immobile trace elements (Zr, Y, Ti, P, REE, etc.) to deduce tectonic environments for volcanics and have developed a variety of discriminant diagrams (Pearce & Cann, 1973; Pearce & Norry, 1979; Pearce, 1982) (Fig. 12). The felsic dyke suite samples plot in the volcanic arc field of Pearce, Harris & Tindle (1984) (Fig. 12a), and are in common with the A-type post-orogenic granite field (Whalen, Currie & Chappell, 1987) characteristic of the within-plate tectonic setting. El-Sayed (2005) similarly suggested a within-plate tectonic setting for emplacement of felsic dykes, exhibiting subduction-related geochemical signatures from the southwest Sinai. Only the mafic dykes are plotted on diagrams that were intended for mafic lavas (Fig. 12b, c, d, f, h). The mafic dyke samples plot in the volcanic island arc and calc-alkaline basalt fields (Fig. 12b–d). The felsic and mafic dykes plot in the destructive plate basalt field (Fig. 12e). The generation of the Wadi Hawashiya dykes in a continental island arc environment is confirmed by the Zr v. Zr/Y and Ti/Y v. Zr/Y plots (Fig. 12f, h) of Pearce & Norry (1979) and $K_2O–TiO_2–P_2O_5$ ternary plot of Pearce, Gorman & Birkett (1975) (Fig. 12g). Moreover, the high contents of Rb, K and $Ta/Yb > 0.1$ for the investigated mafic and felsic dykes rule out an origin from intra-oceanic arc systems (Pearce, 1982). Because the mafic dykes traverse post-collision or within-plate younger granites, the same anorogenic within-plate environment is strongly suggested for the mafic dykes.

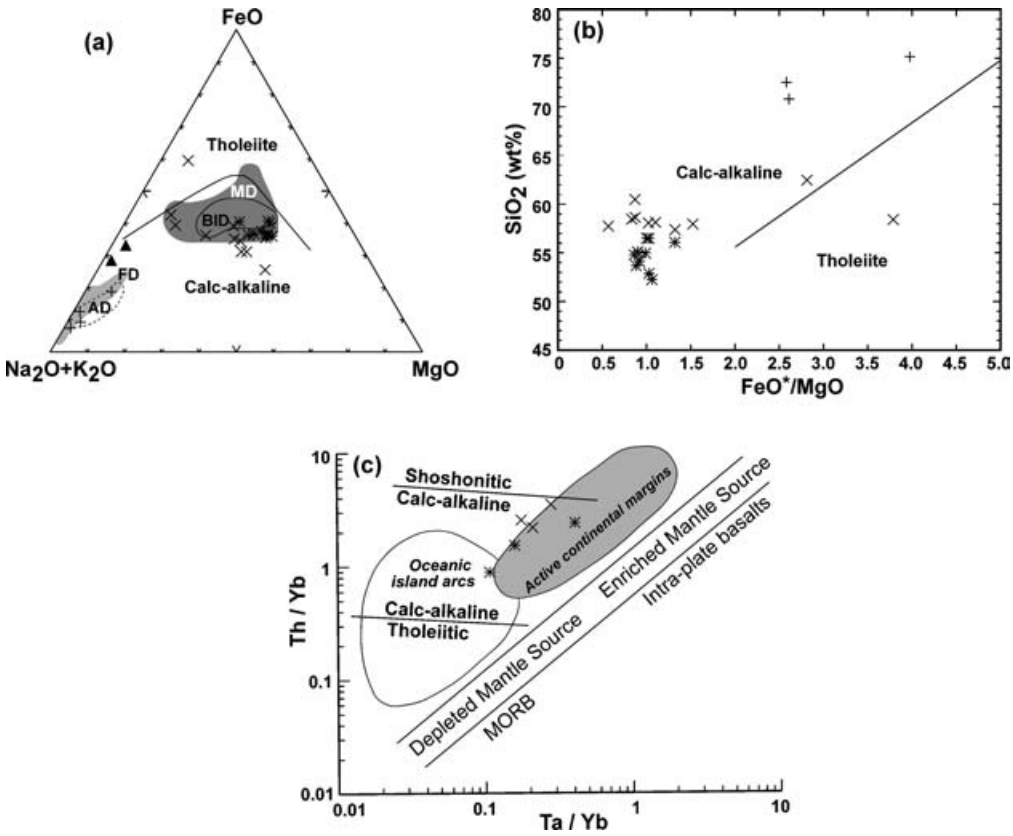

Figure 9. Magma type of Wadi Hawashiya dykes deduced from (a) Alk–FeO*–MgO diagram (Irvine & Baragar, 1971), (b) FeO*/MgO v. SiO_2 diagram (Miyashiro, 1974) and (c) Ta/Yb v. Th/Yb binary diagram (Pearce, 1982). FeO* – total iron as FeO. Compared fields of mafic (MD) and felsic (FD) dykes from the north Eastern Desert (Stern, Sellers & Gottfried, 1988) and of basic-intermediate (BID) and acidic (AD) dykes from Southern Sinai (Iacumin *et al*. 1998). Symbols as in Figure 6.

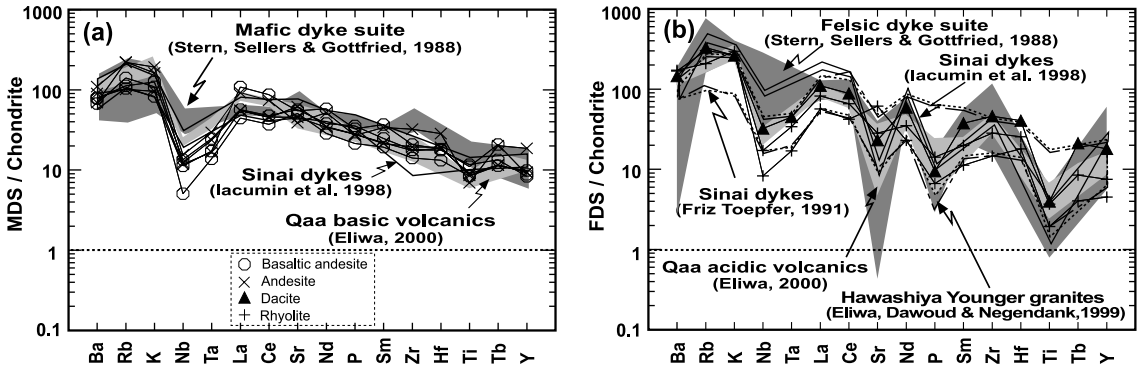

Figure 10. Spider diagrams for Wadi Hawashiya dykes; (a) basaltic andesites (samples 212, 245, 200) and andesites (samples 254, 268, 281) and (b) dacites (sample 214) and rhyolites (samples 271, 222). MDS – mafic dyke suite; FDS – felsic dyke suite. Normalizing values are from Thompson, Hendry & Parry (1984).

8.b. Petrogenesis

Stern, Sellers & Gottfried (1988) classified the north Eastern Desert dykes into mafic dykes (basalt-andesite, 49–66 % SiO_2) having a calc-alkaline nature, and felsic dykes (mainly rhyolites, 70–78 % SiO_2) with alkaline affinities. Basalts are thought to be generated from mantle, and andesites from hydrous melting of garnet peridotite or eclogite, while fractionation processes were responsible for the formation of the rhyolites (Stern, Sellers & Gottfried, 1988). Friz Töpfer (1991) mentioned that the Wadi El Sheikh dykes, Sinai, are calc-alkaline and exhibit subduction-related features, although these dykes were emplaced in an extensional tectonic setting. He suggested that the calc-alkaline basaltic magma was generated in the subcontinental lithosphere which maintained the previous subduction-related geochemical signatures for a long period after

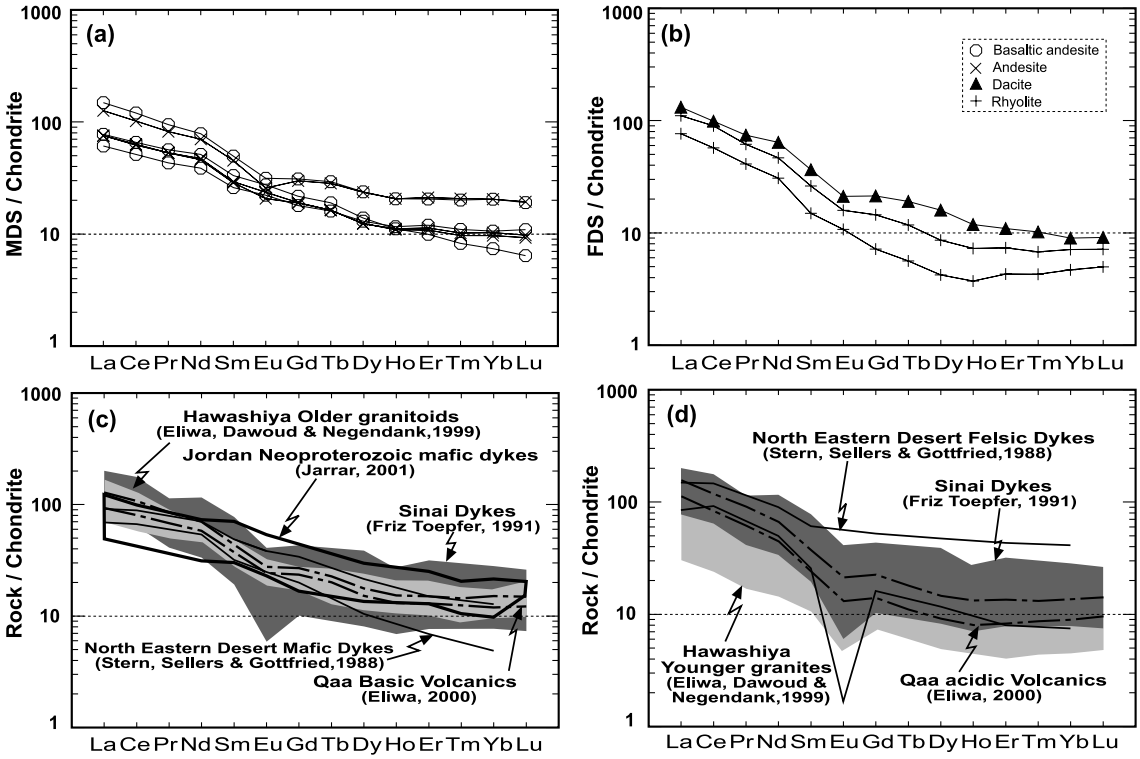

Figure 11. Chondrite-normalized REE patterns of Wadi Hawashiya dykes. (a) Basaltic andesites and andesites, (b) dacites and rhyolites and (c, d) different REE patterns for comparison. MDS – mafic dyke suite, FDS – felsic dyke suite. Normalizing values are from Evensen, Hamilton & O'Nions (1978).

the end of subduction. He also suggested that the more acidic varieties were derived from this basaltic melt via fractional crystallization. Iacumin *et al*. (1998) ruled out the fractionation model for the evolution of both tholeiitic and calc-alkaline felsic dykes.

Wadi Hawashiya dykes resemble the second group of Egyptian dykes (Hassan & Hashad, 1990), which range from basalt to rhyolite in composition, possess calc-alkaline to alkaline affinity and span the time from the older granitoids to the younger granites. The study dykes range from basaltic andesites to rhyolites through andesites (more abundant) and dacites. They are of calc-alkaline affinities and display subduction-related geochemical signatures.

The ratios between the highly incompatible elements (e.g. K/Ba, Ba/La, Nb/La and Ba/Nb) are not significantly affected by fractional crystallization and reflect their original concentrations in the source magmas (Saunders, Norry & Tarney, 1988). Most of these ratios for Wadi Hawashiya dykes completely overlap between the different rock suites. This overlap and similarity for the mafic and felsic dykes may be an argument in favour of fractionation of mafic and felsic melts.

The felsic dyke suite is composed of high-K calc-alkaline rocks with moderate to low Mg number (13–41). The spider diagrams of the felsic dykes are characterized by well-developed Nb–Ta depletion and Sr, P and Ti troughs and LILE enrichment. The negative Nb anomaly in the calc-alkaline rocks is typical of mantle-derived magmas (Holm, 1985), as well as subduction-related calc-alkaline rocks (Saunders, Norry & Tarney, 1991). The troughs at Sr, P and Ti on the multi-element diagram of the felsic dyke suite are strongly consistent with fractional crystallization of feldspar, apatite and Fe–Ti oxides (or titanite) respectively. The low concentrations of Nb and Ta relative to LILE could be attributed to significant crustal contamination (Wilson, 1989).

The systematic changes of most major and some trace elements with increasing SiO_2 make derivation of rhyolites from dacites via crystal fractionation likely. However, the higher Mg number in rhyolites (20–41) than in dacites (13–17) and total absence of or insignificant negative Eu anomalies in rhyolites ($Eu/Eu^* = 0.82–1.04$) compared to that in dacites ($Eu/Eu^* = 0.75$), in addition to the higher bulk REE contents in dacites than in rhyolites, strongly exclude the derivation of rhyolites from dacites by fractional crystallization of the same magma.

The Hawashiya younger granites, which are strongly similar to the felsic dykes in their geochemical features, have been suggested to be derived from a magma generated by partial melting of crustal lithospheric material (or a volcanic arc protolith) at the initial stage of extension (Eliwa, Dawoud & Negendank, 1999). Therefore, we suggest that the felsic dyke suite could be

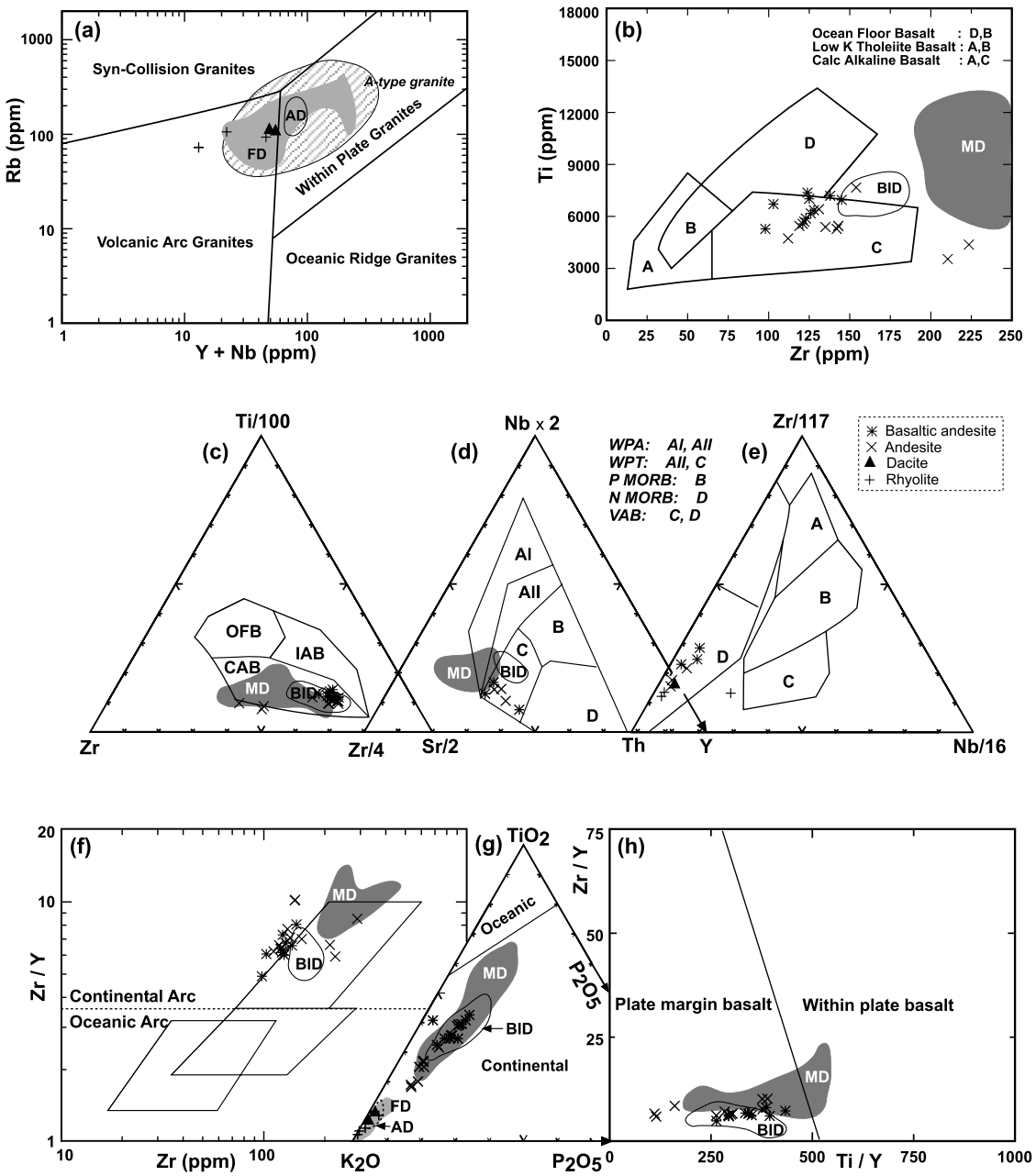

Figure 12. (a) Tectonic discrimination Y + Nb v. Rb diagram (Pearce, Harris & Tindle, 1984); the field of the A-type granite is from Whalen, Currie & Chappell (1987). (b) Ti v. Zr binary diagram (Pearce & Cann, 1973), (c) Zr–Ti/100–Sr/2 ternary diagram (Pearce & Cann, 1973), (d) Zr/4–Nb × 2–Y ternary diagram (Meschede, 1986), (e) Th–Zr/117–Nb/16 diagram (Wood, 1980), (f) Zr v. Zr/Y binary diagram (Pearce & Norry, 1979), (g) K_2O–TiO_2–P_2O_5 ternary diagram (Pearce, Gorman & Birkett, 1975) and (h) Zr/Y v. Ti/Y binary diagram (Pearce & Norry, 1979). Only basaltic andesites and andesites are plotted on the diagrams (b, c, d, f, h). Compared fields of mafic (MD) and felsic (FD) dykes from the north Eastern Desert (Stern, Sellers & Gottfried, 1988) and of basic-intermediate (BID) and acidic (AD) dykes from Southern Sinai (Iacumin *et al*. 1998). OFB – ocean floor basalt, IAB – island arc basalt, CAB – calc-alkali basalt, VAB – volcanic arc basalt, N-MORB – normal mid-oceanic ridge basalt, P-MORB – primitive mid-oceanic ridge basalt, WPA – within-plate alkali basalt, WPT – within-plate tholeiite basalt. Symbols as in Figure 6.

the surface manifestation of the younger granite magma or a similar magma. Hence, the magma, generated by partial melting of crustal lithospheric rocks, seems to be the most suitable and plausible source for the gener–ation of the felsic dykes. This can be further confirmed by whole rock Rb–Sr age of 577 ± 6 Ma for the Wadi younger Hawashiya granites (Stern & Hedge, 1985), which is relatively the same or close to the age of 591 ± 9 Ma given by Stern & Manton (1987) for equivalent Feiran dykes in Sinai.

The mafic dyke suite displays calc-alkaline affinity with Nb–Ta depletion, a slightly deep Ti trough and LILE and LREE enrichment, features characteristic of a subduction-related setting. Both basaltic andesites and

Table 6. Results of closed system fractionation least–square modelling from basaltic andesite to andesite

Oxides	Fractionating phases				Observed daughter (281)*	Observed parent (200)*	Calculated parent
	Plagioclase	Amphibole	Clinopyroxene	Magnetite			
SiO_2	57.35	47.89	48.19	0.10	62.49	56.10	56.11
TiO_2	0.00	0.71	0.92	19.42	0.73	1.23	1.42
Al_2O_3	27.48	6.79	4.59	1.39	15.64	15.37	15.32
FeO	0.13	13.30	8.54	71.50	6.60	8.58	8.53
MnO	0.00	0.46	0.15	2.29	0.11	0.13	0.22
MgO	0.01	15.25	14.42	0.06	2.11	5.84	5.87
CaO	7.09	11.49	21.21	–	3.64	5.97	5.94
Na_2O	6.67	1.17	0.30	–	4.20	3.66	3.80
K_2O	0.89	0.34	0.01	–	2.82	1.84	1.61

The compositions of amphibole, plagioclase, clinopyroxene and magnetite are the actual electron microprobe analyses of the present phenocrysts. Fractional crystallization is 35% and the fractionating phases are: 55 % (plagioclase), 30 % (amphibole), 4 % (clinopyroxene), (11 % magnetite). Sum of squares (R^2) is 0.18. Parent = 65 % (daughter) + 19 % (plagioclase) + 11 % (amphibole) + 1 % (clinopyroxene) + 4 % (magnetite). * Sample number.

andesites show overlap in the major and some trace element contents (e.g. Sr, Zr, Rb, Y). The bulk REE contents of andesites overlap with that of some basaltic andesites, but few samples display an increase in the REE concentration from basaltic andesites to andesites, that is, with increasing SiO_2 (wt%). This supports the derivation of andesites from basaltic andesites by fractional crystallization processes.

To test whether fractional crystallization can account for the compositional variability of the mafic suite, the least-squares approximation method of Le Maitre (1981) was applied to the major elements and the results are presented in Table 6. According to the phenocrysts in andesites, the fractionated mineral assemblages are plagioclase, amphibole, clinopyroxene and magnetite. The chemical composition of the fractionated phases used in modelling is given in Table 6. The modelling results show that andesite (sample no. 281) is derived by about 35 % fractional crystallization of plagioclase (19), amphibole (11), clinopyroxene (1) and magnetite (4) from basaltic andesite (sample no. 200). The percentages of the fractionated phases obtained from least-squares fractionation modelling are used in the Rayleigh crystal fractionation model of the rare earth elements (REE). The Rayleigh REE modelling (Table 7) shows that andesite was produced after approximately 40–45 % fractional crystallization of basaltic andesite melt. The differences between calculated and observed concentrations of some rare earth elements for andesites are mainly due to uncertainties in the partition coefficients (K_D), and changes in the composition of phenocrysts and solid-solution minerals during fractional crystallization process. The partition coefficients used in modelling are given in Table 8.

Basaltic magmas can be produced by direct melting of the upper mantle, either during major lithospheric extension (Morgan, 1981; Richards, Duncan, & Courtillot, 1989; Campbell & Griffiths, 1990), or by the interaction between continental materials and mantle–derived magma (Duncan, Erlank, & Marsh, 1984; Ellam & Cox, 1989). Where there is no evidence for magma mixing, it is suggested that basaltic andesites and andesites were derived from basic magma generated by partial melting of mantle which originally inherited and still maintained the geochemical subduction-related signatures for a long period after the subduction process stopped. The moderate to high contents of compatible elements such as Cr (up to 250 ppm) and Ni (up to 141 ppm), and Mg number (54–76) support the generation of mafic dykes magma from mantle (Mg no. of mantle > 65), and also indicate a relative primitive composition of mantle magma (Frey, Green & Roy,

Table 7. Results of the rare earth elements Rayleigh fractional crystallization modelling from basaltic andesite to andesite

	Observed parent (200)*	Observed daughter (281)*	40 % fractional crystallization	45 % fractional crystallization
La	19.00	30.80	27.82	29.69
Ce	41.90	65.10	61.39	65.52
Pr	5.45	7.89	7.77	8.25
Nd	24.30	33.30	33.46	35.33
Sm	5.12	6.97	6.55	6.82
Eu	1.59	1.49	1.89	1.95
Gd	4.44	6.08	5.50	5.70
Dy	3.53	6.00	4.05	4.41
Er	1.65	3.51	1.91	1.96
Yb	1.22	3.38	1.57	1.64
Lu	0.16	0.49	0.21	0.22

* Sample number.

Table 8. Partition coefficients used in the rare earth elements fractional crystallization modelling (after Art, 1976 and Gill, 1981)

	Hornblende	Plagioclase	Clinopyroxene	Magnetite
La	0.440	0.180	0.288	0.10
Ce	0.540	0.120	0.303	0.11
Pr	0.750	0.097	0.341	0.13
Nd	1.000	0.081	0.379	0.13
Sm	1.490	0.067	0.476	0.15
Eu	1.500	0.340	0.354	0.10
Gd	1.700	0.063	0.561	0.12
Dy	2.200	0.055	0.663	0.14
Er	2.100	0.063	0.706	0.16
Yb	1.400	0.067	0.719	0.17
Lu	1.300	0.060	0.719	0.19

Table 9. Some significant elemental ratios of Wadi Hawashiya dykes and other dyke suites from north Eastern Desert and southern Sinai

Element ratio	Ce/Nb		Zr/Y		Zr/Nb		K/Rb		Y/Nb		La/Nb		La/Zr		$(La/Sm)_N$		$(La/Lu)_N$		$(La/Yb)_N$		Eu/Eu*	
rock type	Mean	SD	Mean	SD	Mean	SD	Mean	SD	Mean	SD	Mean	SD	Mean	SD	Mean	SD	Mean	SD	Mean	SD	Mean	SD
Mafic dykes	12.76	4.72	6.99	1.32	36	10	311	51	5.82	2.83	5.92	2.23	0.16	0.04	2.61	0.25	7.98	2.24	7.48	1.68	0.91	0.14
Felsic dykes	9.20	3.51	9.62	2.14	32	3	381	131	2.93	0.38	4.58	1.79	0.14	0.05	4.31	0.77	14.23	2.05	15.51	0.86	0.87	0.15
NED-MD	4.39	0.61	11.71	5.27	22	3	316	67	2.01	0.46	1.84	0.33	0.08	0.01	2.22	0.43	–	–	9.50	4.74	0.97	0.06
NED-FD	3.31	2.45	6.27	4.06	12	11	303	237	1.63	0.58	1.40	1.23	0.12	0.03	2.67	1.61	–	–	8.11	6.81	0.34	0.38
Sinai Dykes	6.39	0.66	7.42	2.27	18	2	316	13	2.59	0.79	2.75	0.44	0.15	0.02	2.95	0.85	9.23	1.99	8.84	2.03	0.71	0.22
Sinai-1 Dykes	8.79	2.58	8.40	3.33	18	3	–	–	2.34	0.66	4.40	1.42	0.24	0.05	4.85	1.22	21.38	12.3	21.36	11.63	0.70	0.06
OIB	1.67	–	9.66	–	6	–	387	–	0.60	–	0.77	–	0.13	–	0.02	–	12.60	–	11.49	–	1.05	–
MORB	3.34	–	57.32	–	25	–	853	–	0.44	–	1.11	–	0.04	–	0.10	–	0.72	–	0.71	–	0.96	–
PM	–	–	2.5	–	16	–	394	–	0.03	–	1.00	–	0.06	–	–	–	–	–	–	–	–	–
ALC	–	–	2.8	–	19	–	527	–	0.00	–	1.80	–	0.10	–	–	–	–	–	–	–	–	–
UC	–	–	4.5	–	10	–	316	–	0.06	–	0.90	–	0.09	–	–	–	–	–	–	–	–	–
LC	–	–	4.9	–	12	–	329	–	0.04	–	1.85	–	0.15	–	–	–	–	–	–	–	–	–

NED-MD and NED-FD – Mafic and felsic dykes from north Eastern Desert (Stern, Sellers & Gottfried, 1988); Sinai dykes – Wadi El-Sheikh (S1) dykes (Friz Toepfer, 1991); Sinai-1 dykes – Sinai dykes (Iacumin *et al*. 1998). PM – Primitive mantle (Sun & McDonough, 1989); ALC – Arabian lower crust (McGuire & Stern, 1993). UC – upper crust, LC – lower crust (Kempton *et al*. 1991).

1978). The similar negative Nb, Ti and Eu anomalies of most mafic dykes suggest a role of fractional crystallization in their evolution. The LILE and LREE enrichment and the Nb trough may be attributed to melts from metasomatically enriched mantle sources (Richardson *et al*. 1982). This conclusion agrees with the previous models for the petrogenesis and evolution of dykes in the north Eastern Desert (Stern, Sellers & Gottfried, 1988) and Sinai (Friz Töpfer, 1991; El-Sayed, 2005). Friz Töpfer (1991) ascribed the calc-alkaline and subduction-related features for Wadi El Sheikh dykes to the change from plate destruction to extensional tectonism and their magmas were generated in subcontinental lithosphere which still retains the characteristics of its subduction-related magmatic history. According to Tarney (1992), subcontinental lithosphere was suggested to be the dominant source component of most dyke swarm magmas. Many studies (Rogers *et al*. 1987; Thirwall, 1988; Sloman, 1989) confirm the ability of mantle to retain subduction-related geochemical signatures for substantial periods of time after cessation of subduction.

8.c. Genetic relationship and comparison of the studied dykes with other dykes from adjacent areas and countries

The field observations and cross-cutting relationships of the felsic dykes with mafic dykes indicate that it is very unlikely that felsic dykes were derived from mafic dykes. Moreover, the chemical differences and variation diagrams argue against this derivation by fractional crystallization. This agrees with the suggestion of two different magma types for the generation of the mafic and felsic dykes from the Eastern Desert (Stern and Gottfried, 1986) and Sinai (El Sayed, 2005). On the spider diagrams (Fig. 10a, b), the presumably equivalent dykes from the north Eastern Desert (Stern, Sellers & Gottfried, 1988; Eliwa, 2000) and Sinai (Friz Töpfer, 1991; Iacumin *et al*. 1998) show similarity to the studied dykes.

Figure 11c, d displays the REE patterns of the Hawashiya older and younger granitoid rocks (Eliwa, Dawoud & Negendank, 1999), the Qaa basic and felsic volcanic rocks (Eliwa, 2000), the north Eastern Desert mafic and felsic dykes (Stern, Sellers & Gottfried, 1988) and the Sinai dykes (Friz Töpfer, 1991). The REE patterns of the mafic dyke suite are comparable to those of the host Hawashiya older granitoids (Eliwa, Dawoud & Negendank, 1999), S1 Sinai dykes (Friz Töpfer, 1991), Qaa basic Dokhan Volcanics (Eliwa, 2000), and with the north Eastern Desert mafic dykes (Stern, Sellers & Gottfried, 1988) (Fig. 11c, d). The REE patterns of the felsic dykes are similar to that of the host Hawashiya younger granites (Eliwa, Dawoud & Negendank, 1999), S1 Sinai dykes (Friz Töpfer, 1991), Qaa felsic Dokhan Volcanics (Eliwa, 2000) and north Eastern Desert felsic volcanics (Stern, Sellers & Gottfried, 1988), but the felsic dykes do not show significant negative Eu anomalies. Therefore, the felsic dykes are probably surface manifestations of the same magmatic phase that produced the Hawashiya younger granites. In Table 9, most ratios of both suites show a close similarity to those of S1 Sinai dykes (Friz Töpfer, 1991), some ratios are similar to those of the mafic and felsic dykes from the north Eastern Desert (Stern, Sellers & Gottfried, 1988); very few ratios are close to those for the lower and upper crust (Kempton *et al*. 1991), and no ratios are close to those of primitive mantle (Sun & McDonough, 1989).

Jarrar (2001) studied the Late Neoproterozoic mafic dykes from southern Jordan, which exhibit considerable similarities to the studied dykes (Fig. 11c). He suggested that these dykes were generated in an extensional continental tectonic setting, were crystallized at 1050–800 °C and were derived by 5 % modal patch partial melting metasomatized lithospheric mantle (phlogopite-bearing spinel lherzolite). Neoproterozoic

(565 ± 7 Ma) composite dykes from southwestern Jordan studied by Jarrar *et al*. (2004) exhibit a great similarity to the studied dykes, where the geochemical data do not favour a fractional crystallization relationship between the felsic and mafic dykes. They suggested that these dykes were generated in an extensional continental tectonic setting, and their basic mantle magma underwent an extensive fractional crystallization, which supplied the necessary heat for partial melting (5–10%) of the lower crust. The resultant melt mixed with the fractionating mantle mafic magma and gave rise to the mafic dyke members. Further partial melting of the lower crust (up to 30 %) produced a felsic melt, which upon fractional crystallization gave rise to the felsic dykes members.

9. Summary

The present study results in the following conclusions:

(1) The Wadi Hawashiya dykes comprise mafic (basaltic andesites and andesites) and felsic dyke suites (dacites and rhyolites) that intrude Neoproterozoic granites and granitoids. The mafic dykes are younger than the felsic dykes.

(2) All Hawashiya dykes are parallel to subparallel, dip vertically to very steeply (90–75°) and trend in a NE–SW direction, namely N45° E in most areas to N52° E in the southern part of the area.

(3) Both the felsic and mafic dyke suites show calc-alkaline affinities, according to major element contents and microprobe data, of clinopyroxene and biotite.

(4) The composition of clinopyroxenes is augite in basaltic andesites and varies from augite to diopside in andesites. Basaltic andesites crystallized at temperatures between 950 and 1220 °C, while andesites crystallized between 860 and 1170 °C.

(5) Amphibole composition from basaltic andesites and andesites ranges mainly from magnesio-hornblende and actinolitic hornblende to magnesio-hastingsite and indicates a low-pressure environment.

(6) Normalized multi-element diagrams of the Hawashiya dykes display an overall enrichment of the incompatible elements and HFSE relative to the chondrite primitive melt. The mafic dyke suite is characterized by a Nb–Ta trough and a weak negative Ti anomaly, while the felsic dyke suite is characterized also by a Nb–Ta trough and negative Sr, P and Ti anomalies.

(7) The felsic dykes show a strongly fractionated LREE ($La_N/Yb_N = 14.6–16.3$, av. 15.5) compared with the mafic dykes ($La_N/Yb_N = 5.8–10.5$, av. 7.5).

(8) The magma source of the felsic dyke suite can be derived essentially from crustal rocks by high degree of partial melting.

(9) The mafic dyke suite magma(s) were generated from lithospheric mantle, which had enriched with the subducted slab-derived melts or fluids. The geochemical trends together with the major and rare earth element modelling suggest that the andesites were derived from the basaltic andesites by approximately 35 to 45 % fractional crystallization of the mineral assemblage comprising plagioclase, amphibole, clinopyroxene and magnetite.

Acknowledgements. The authors thank D. A. Conte and Mr G. Aurisicchio, C. N. R., Roma La Sapienza, Roma, Italy, for carrying out XRF analyses and to Mr L. Martarelli at the same institute for microprobe analyses. The authors are indebted to Prof. Dr J. F. Negendank, GFZ Potsdam, Germany, for entertaining discussions on the dykes' petrogenesis. We would also like to thank the referees, Prof. R. Stern and Prof. G. Jarrar, for their valuable comments that greatly contributed to improvement of the manuscript. We extend our thanks to Dr D. Pyle for his editorial efforts which further improved the manuscript.

References

Abdel Rahman, A. M. 1994. Nature of biotites from alkaline, calc-alkaline and peraluminous magmas. *Journal of Petrology* **35**, 525–41.

Arth, J. G. 1976. Behavior of trace elements during magmatic processes – a summary of theoretical models and their applications. *Journal of Research of the U.S. Geological Survey* **4**, 41–7.

Berhe, S. M. 1990. Ophiolites in northeast and east Africa: Implications for Proterozoic crustal growth. *Journal of the Geological Society, London* **147**, 41–57.

Campbell, I. H. & Griffiths, R. W. 1990. Implications of mantle plume structure for the evolution of flood basalts. *Earth and Planetary Science Letters* **99**, 79–93.

Condie, K. C. 1990. Growth and accretion of continental crust: Inferences based on Laurentia. *Chemical Geology* **93**, 183–94.

Deer, W. A., Howie, R. A. & Zussman, J. 1966. *An introduction to the rock-forming minerals*. Longman Group UK Ltd.

Dixon, T. H. & Golombek, M. P. 1988. Late Precambrian crustal accretion rates in northeast Africa and Arabia. *Geology* **16**, 991–4.

Duncan, A. R. 1987. The Karoo igneous province: a problem area for inferring tectonic setting from basalt geochemistry. *Journal of Volcanology and Geothermal Research* **32**, 13–34.

Duncan, A. R., Erlank, A. J. & Marsh, J. S. 1984. Regional geochemistry of the Karoo igneous province. In *Petrogenesis of the Volcanic Rocks of the Karoo Province* (ed. A. J. Erlank), pp. 355–88. Geological Society of South Africa, Special Publication no. 13.

Eliwa, H. A. 2000. Petrology, Geochemistry, Mineral Chemistry and Petrogenesis of Samr El-Qaa Volcanics, North Eastern Desert, Egypt. *Scientific Journal Faculty Science, Minufiya University* **XIV**, 1–45.

Eliwa, H. A., Dawoud, M. & Negendank, J. F. W. 1999. Pan-African Magmatism: Geochemistry, mineral chemistry and petrogenesis of granitoid rocks of Wadi Hawashiya area, North Eastern Desert, Egypt. *4th International Conference on Geochemistry, Alexandria University, Egypt*, 47–68.

Ellam, R. M. & Cox, K. G. 1989. A Proterozoic lithospheric source for Karoo magmatism: Evidence from the Nuanetsi picrites. *Earth and Planetary Science Letters* **92**, 207–18.

EL-RAMLY, M. F. & HERMINA, M. H. 1978. *Geological map of the Aswan quadrangle, Egypt*. Egyptian Geological Survey Mining Authority.

EL-SAYED, M. M. 2005. Geochemistry and petrogenesis of the post-orogenic bimodal dyke swarms in NW Sinai, Egypt: constraints on the magmatic-tectonic processes during the late Precambrian. *Chemie der Erde* (in press).

EVENESEN, N. M., HAMILTON, P. J. & O'NIONS, R. K. 1978. Rare earth abundances in chondritic meteorites. *Geochimica et Cosmochimica Acta* **42**, 1199–1212.

EWART, A. 1982. The mineralogy and petrology of Tertiary–Recent orogenic volcanic rocks with special reference to the andesite-basaltic compositional range. In *Andesites, Orogenic andesites and related rocks* (ed. R. S. Thorpe), pp. 25–87. Chichester, New York: John Wiley and Sons.

FREY, F. A., GREEN, D. H. & ROY, S. D. 1978. Integrated models of basalts petrogenesis: A study of quartz tholeiites to olivine melilites from south western Australia using geochemical and experimental data. *Journal of Petrology* **19**, 463–513.

FRIZ TÖPFER, A. 1991. Geochemical characterization of Pan-African dyke swarms in southern Sinai: from continental margin to intraplate magmatism. *Precambrian Research* **49**, 281–300.

GILL, J. B. 1981. *Orogenic Andesites and Plate Tectonics*. Berlin: Springer-Verlag, 389 pp.

GREENWOOD, H. R., HADLEY, D. G., ANDERSON, R. E., FLECK, R. J. & SCHMIDT, D. L. 1976. Late Proterozoic cratonization in southwestern Saudi Arabia. *Philosophical Transactions of the Royal Society of London* **280**A, 517–27.

HASSAN, M. A. & HASHAD, A. H. 1990. Precambrian of Egypt. *In The Geology of Egypt* (ed. R. Said), pp. 201–45. Rotterdam, Brookfield: Balkema.

HOFMANN, A. W. 1988. Chemical Differentiation of the Earth: the relationship between mantle, continental crust, and oceanic crust. *Earth and Planetary Science Letters* **90**, 297–314.

HOFMANN, A. W. & STEIN, M. 1994. Episodic crustal growth and mantle evolution. *Mineralogical Magazine* **58A**, 420–1.

HOLM, P. E. 1985. The geochemical fingerprints of different tectonic magmatic environments using hydromagmaphile elements abundances of tholeiitic basaltic andesites. *Chemical Geology* **51**, 303–23.

IACUMIN, M., MARZOLI, A., EL METWALLY A. A. & PICCIRILILO, E. M. 1998. Neoproterozoic dyke swarms from southern Sinai (Egypt): geochemistry and petrogenetic aspects. *Journal of African Earth Sciences* **26**(1), 49–64.

IRVINE, T. N. & BARAGAR, W. R. A. 1971. A guide to the chemical classification of the common volcanic rocks. *Canadian Journal of Earth Sciences* **8**, 523–48.

JARRAR, G. 2001. The youngest Neoproterozoic mafic dyke suite in the Arabian Shield: mildy alkaline dolerites from South Jordan – their geochemistry and petrogenesis. *Geological Magazine* **138**, 309–33.

JARRAR, G., SAFFARINI, G., BAUMANN, A. & WACHENDORF, H. 2004. Origin, age and petrogenesis of Neoproterozoic composite dikes from the Arabian–Nubian Shield, SW Jordan. *Geological Journal* **39**, 157–78.

KEMPTON, P. D., HARMON, R. S., HAWKESWORTH, C. J. & MOORBATH, S. 1991. Petrology and geochemistry of lower crustal granulites from the Geronimo volcanic field, southeastern Arizon. *Geochimica et Cosmochimica Acta* **54**, 195–213.

LEAKE, B. E. 1978. Nomenclature of amphiboles. *Mineralogical Magazine* **42**, 533–63.

LE BAS, M. J. 1962. The role of aluminum in igneous clinopyroxenes with relation to their parentage. *American Journal of Science* **260**, 267–88.

LE MAITRE, R. W. 1981. GENMIX – A generalised petrological mixing model program. *Computers and Geosciences* **7**, 229–47.

LE MAITRE, R. W. 1989. *A classification of igneous rocks and glossary of terms*. Oxford: Blackwell, 193 pp.

LETTERRIER, J., MAURY, R. C., THONON, P., GIRARD, D. & MARCHAL, M. 1982. Clinopyroxene composition as a method of identification of the magmatic affinities of paleo-volcanic series. *Earth and Planetary Science Letters* **59**, 139–54.

LINDSLEY, D. H. 1983. Pyroxene thermometry. *American Mineralogist* **68**, 477–93.

LÖFGREN, G. E. 1974. An experimental study of plagioclase crystal morphology: Isothermal crystallization. *American Journal of Science* **274**, 243–73.

MESCHEDE, M. 1986. A method of discriminating between different types of mid-oceanic ridge basalts and continental tholeiites with Nb–Zr–Y diagram. *Chemical Geology* **56**, 207–18.

MIYASHIRO, A. 1974. Volcanic rock series in island arcs and active continental margins. *American Journal of Science* **274**, 321–55.

MORGAN, W. J. 1981. Hotspot tracks and the opening of the Atlantic and Indian oceans. In *The Oceanic Lithosphere* (ed. C. Emiliani), pp. 443–87. New York: Wiley Interscience.

MORIMOTO, N. 1988. The nomenclature of pyroxenes. *Mineralogical Magazine* **52**, 535–50.

NORRISH, K. & HUTTON, J. T. 1969. An accurate X-ray spectrographic method for the analysis of a wide range of geological samples. *Geochimica et Cosmochimica Acta* **33**, 431–53.

PALLISTER, J. S., STACY, J. S., FISCHER, L. B. & PREMO, W. R. 1988. Precambrian ophiolites of Arabia: Geological settings, U–Pb geochronology, Pb-isotope characteristics, and implications for continental accretion. *Precambrian Research* **38**, 1–54.

PEARCE, J. A. 1982. Trace element characteristics of lavas from destructive plate boundaries. In *Andesites* (ed. R. S. Thorpe), pp. 525–48. Chichester: Wiley.

PEARCE, J. A. 1983. Role of the sub-continental lithosphere in magma genesis at active continental margins. In *Continental Basalts and Mantle Xenoliths* (eds C. J. Hawkesworth and M. J. Norry), pp. 230–49. Shiva Publishing Ltd.

PEARCE, J. A. & CANN, J. R. 1973. Tectonic setting of basic volcanic rocks determined using trace element analyses. *Earth and Planetary Science Letters* **19**, 290–300.

PEARCE, J. A., GORMAN, B. E. & BIRKETT, T. C. 1975. The TiO_2–K_2O–P_2O_5 diagram: A method of discriminating between oceanic and non-oceanic basalts. *Earth and Planetary Science Letters* **24**, 419–26.

PEARCE, J. A., HARRIS, N. B. W. & TINDLE, A. G. 1984. Trace element discrimination diagrams for the tectonic interpretation of granitic rocks. *Journal of Petrology* **25**, 956–83.

PEARCE, J. A. & NORRY, M. J. 1979. Petrogenetic implications of Ti, Zr, Y, and Nb variations in volcanic rocks. *Contributions to Mineralogy and Petrology* **69**, 33–47.

RAASE, P. 1974. Al and Ti contents of the hornblende, indicators of pressure and temperature of regional

metamorphism. *Contributions to Mineralogy and Petrology* **45**, 231–6.

RICHARDS, M. A., DUNCAN, R. A. & COURTILLOT, V. E. 1989. Flood basalts and hotspot tracks: Plume heads and trails. *Science* **246**, 103–7.

RICHARDSON, S. H., ERLANK, A. J., DUNCAN, A. R. & REID, D. L. 1982. Correlated Nd, Sr and Pb isotope variations in Walvis Ridge basalt and implications for the evolution of their mantle source. *Earth and Planetary Science Letters* **59**, 327–42.

ROGERS, N. W., HAWKESWORTH, C. J., MATTEY, D. P. & HARMON, R. S. 1987. Sediment subduction and the source of potassium in orogenic leucitites. *Geology* **15**, 451–3.

SAUNDERS, A. D., NORRY, M. J. & TARNEY, J. 1988. Origin of MORB and chemically-depleted mantle reservoirs: trace element constraints. *Journal of Petrology, Special Lithosphere Issue*, 415–45.

SAUNDERS, A. D., NORRY, M. J. & TARNEY, J. 1991. Fluid influence on the trace element compositions of subduction zone magmas. *Philosophical Transactions of the Royal Society of London* **A335**, 337–92.

SCHÜRMANN, H. M. 1966. *The Precambrian of the Gulf of Suez and northern part of Red Sea*. Leiden, Netherlands: E. J. Brill, 404 pp.

SLOMAN, L. E. 1989. Triassic shoshonites from the dolomites of northern Italy, alkaline arc rocks in a strike-slip setting. *Journal of Geophysical Research* **94**, 4655–66.

STERN, R. J. 1985. The Najd-fault system, Saudi Arabia and Egypt: A late Precambrian rift-related transform system? *Tectonics* **4**, 497–511.

STERN, R. J. & GOTTFRIED, D. 1986. Petrogenesis of a Late Precambrian 575–600 Ma bimodal suite in northeast Africa. *Contributions to Mineralogy and Petrology* **92**, 492–501.

STERN, R. J., GOTTFRIED, D. & HEDGE, C. E. 1984. Late Precambrian rifting and crustal evolution in the Northeastern Desert of Egypt. *Geology* **12**, 168–72.

STERN, R. J. & HEDGE, C. E. 1985. Geochronological and isotopic constraints on the Late Precambrian crustal evolution in the Eastern Desert of Egypt. *American Journal of Science* **285**, 97–127.

STERN, R. J. & MANTON, W. I. 1987. Age of Feiran basement rocks, Sinai: implications for Late Precambrian crustal evolution in the northern Arabian–Nubian Shield. *Journal of the Geological Society, London* **144**, 569–75.

STERN, R. J., SELLERS, G. & GOTTFRIED, D. 1988. Bimodal dyke swarms in the North Eastern Desert of Egypt: Significance for the origin of Late Precambrian "A-type" granites in Northern Afro-Arabia. In *The Pan-African belt of Northeast Africa and adjacent areas* (eds S. El-Gaby and R. D. Greiling), pp. 147–79. Braunschweig/Wiesbaden: Friedrich Vieweg & Sohn.

STERN, R. J. & VOEGELI, D. A. 1987. Geochemistry, geochronology, and petrogenesis of a late Precambrian (~590 Ma) composite dike from the North Eastern Desert of Egypt. *Geologische Rundschau* **76**, 325–41.

SUN, C. M. & BERTRAND, J. 1991. Geochemistry of clinopyroxenes in plutonic and volcanic sequences from the Yanbian Proterozoic ophiolites (Sichuan Province, China): Petrogenetic and geotectonic implications. *Schweizerische Mineralogische und Petrographische Mitteilungen* **71**, 243–59.

SUN, S. S. & MCDONOUGH, W. F. 1989. Chemical and isotopic systematics of oceanic basalts: Implications for mantle composition and processes. In *Magmatism in the ocean Basins* (eds A. D. Saunders and M. J. Norry), pp. 313–45. Geological Society of London, Special Publication no. 42.

TARNEY, J. 1992. Geochemistry and significance of mafic dyke swarms in the Proterozoic. In *Proterozoic crustal evolution* (ed. K. C. Condie), pp. 150–79. Amsterdam: Elsevier.

THIRWALL, M. F. 1988. Wenlock to mid-Devonian Volcanism of the Caledonian–Appalachian Orogen. In *The Caledonian–Appalachian Orogen* (eds A. L. Harris and D. J. Fettes), pp. 415–28. Geological Society of London, Special Publication no. 38.

THOMPSON, R. N., HENDRY, G. L. & PARRY, S. J. 1984. An assessment of the relative roles of crust and magma genesis: An elemental approach. *Philosophical Transactions of the Royal Society of London* **310**, 549–90.

WHALEN, J. B., CURRIE K. L. & CHAPPELL, B. W. 1987. A-type granites: geochemical characteristics, discrimination and petrogenesis. *Contributions to Mineralogy and Petrology* **95**, 407–19.

VAIL, J. R. 1970. Tectonic control of dikes and related irruptive rocks in eastern Africa. In *African magmatism and tectonics* (eds T. N. Clifford and I. G. Gass), pp. 337–54. Edinburgh: Oliver and Boyd.

WILSON, M. 1989. *Igneous Petrogenesis*. London: Unwin Hyman Ltd, 466 pp.

WINCHESTER, J. A. & FLOYD, P. A. 1977. Geochemical discrimination of different magma series and their differentiation products using immobile elements. *Chemical Geology* **20**, 325–43.

WOOD, D. A. 1980. The application of a Th-Hf-Ta diagram to problems of tectonomagmatic classification and to establishing the nature of crustal contamination of basaltic lavas of the British Tertiary volcanic povince. *Earth and Planetary Science Letters* **50**, 11–30.